regulated by STAT under the control of IL-3 in Baf-3 cells [21]. These data indicate a similar rate of transcription initiation of the *Bim* gene in Baf-3 cells cultured in the presence or absence of IL-3.

Our data suggest that, unlike NGF in PC12 cells, IL-3 does not induce the expression of *Bim* mRNA at the level of the initiation of transcription in Baf-3 cells. Cytokines have been shown to regulate the function of Bim through various mechanisms, including transcriptional regulation, proteasome-dependent protein degradation, control of subcellular localization, and phosphorylation. The contribution of each distinct mechanism of regulation differs between cell types, indicating that mammalian cells have evolved the suitable control mechanism for this important determination factor of their own fate. Indeed, our preliminary data suggests that IL-3 regulates the stability of *Bim* mRNA in Baf-3 cells (data not shown). We are currently investigating the detailed molecular mechanism of the regulation of *Bim* mRNA stability in our laboratory.

References

1. Miyajima A, Ito Y & Kinoshita T (1999) Int. J. Hematol. 69: 137–146.
2. Kinoshita T, Shirouzu M, Kamiya A, Hashimoto K, Yokoyama S & Miyajima A (1997) Oncogene 15: 619–627.
3. Kuribara R, Kinoshita T, Miyajima A, Shinjyo T, Yoshihara T, Inukai T, Ozawa K Look AT & Inaba T (1999) Mol. Cell. Biol. 19: 2754–2762.
4. Cory S, Huang DC & Adams JM (2003) Oncogene 22: 8590–8607.
5. O'Connor L, Strasser A, O'Reilly LA, Hausmann G, Adams JM, Cory S & Huang DC (1998) EMBO J. 17: 384–395.
6. Hsu SY, Lin P & Hsueh AJ (1998) Mol. Endocrinol. 12: 1432–1440.
7. Shinjyo T, Kuribara R, Inukai T, Hosoi H, Kinoshita T, Miyajima A, Houghton PJ, Look AT, Ozawa K & Inaba T (2001). Mol. Cell. Biol. 21: 854–864.
8. Dijkers PF, Medemadagger RH, Lammers JJ, Koenderman L & Coffer PJ (2000) Curr. Biol. 10: 1201–1204.
9. Bouillet P, Metcalf D, Huang DCS, Tarlinton DM, Kay TWH, Koentgen F, Adams JM & Strasser A (1999) Science 286: 1735–1738.
10. Biswas SC & Greene LA (2002) J. Biol. Chem. 277: 49511–49516.
11. Putcha GV, Moulder KL, Golden JP, Bouillet P, Adams JA, Strasser A & Johnson EM (2001) Neuron 29: 615–628.
12. Whitfield J, Neame SJ, Paquet L, Bernard O & Ham J (2001) Neuron 29: 629–643.
13. Ley R, Balmanno K, Hadfield K, Weston CR & Cook SJ (2003) J. Biol. Chem. 278: 18811–18816.
14. Akiyama T, Bouillet P, Miyazaki T, Kadono Y, Chikuda H, Chug U, Fukuda A, Hikita A, Seto H, Okada T, Inaba T, Sanjay A, Baron R, Oda H, Nakamura K, Strasser A & Tanaka S (2003) EMBO J. 22: 6653–6664.
15. Puthalakath H, Huang DC, O'Reilly LA, King SM & Strasser A (1999) Mol. Cell 3: 287–296.
16. Lei K & Davis RJ (2003) Proc. Natl. Acad. Sci. USA 100: 2432–2437.
17. Yamaguchi T, Okada T, Takeuchi T, Tonda T, Ohtaki M, Shinoda S, Masuzawa T, Ozawa K & Inaba T (2003) Gene Ther. 10: 375–385.
18. Kuribara R, Honda H, Matsui H, Shinjyo T, Inukai T, Sugita K, Nakazawa S, Hirai H, Ozawa K & Inaba T (2004) Mol. Cell. Biol. 24: 6172–6183.
19. Gilley J, Coffer PJ & Ham J (2003) J. Cell. Biol. 162: 613–622.
20. Bouillet P, Zhang LC, Huang DC, Webb GC, Bottema CD, Shore P, Eyre HJ, Sutherland GR & Adams JM (2001) Mamm. Genome 12: 163–168.
21. Socolovsky M, Fallon AE, Wang S, Brugnara C & Lodish HF (1999) Cell 98: 181–191.

Available online at www.sciencedirect.com

SCIENCE DIRECT®

Brain Research 1050 (2005) 15–26

BRAIN RESEARCH

www.elsevier.com/locate/brainres

Research Report

Neuroprotective effects of erythropoietin on glutamate and nitric oxide toxicity in primary cultured retinal ganglion cells

Makiko Yamasaki[a], Hiromu K. Mishima[a,*], Hidetoshi Yamashita[b], Kenji Kashiwagi[c], Kazuhiko Murata[a], Atsushi Minamoto[a], Toshiya Inaba[d]

[a]*Department of Ophthalmology and Visual Science, Graduate School of Biomedical Sciences, Hiroshima University, 1-2-3 Kasumi, Minami-ku, Hiroshima 734-8551, Japan*
[b]*Department of Ophthalmology and Visual Science, Yamagata University School of Medicine, Japan*
[c]*Department of Ophthalmology, University of Yamanashi Faculty of Medicine, Japan*
[d]*Department of Molecular Oncology, Research Institute for Radiation Biology and Medicine, Hiroshima University, Japan*

Accepted 3 May 2005

Abstract

Erythropoietin receptor (EpoR) is expressed in the central nervous system (CNS), however, no clear consensus has been obtained whether Epo acts as a prosurvival factor in neurons. Because retinal ganglion cell (RGC) death is a common cause of reduced visual function in several ocular diseases, we explored whether Epo might potentially be beneficial in protecting RGCs from glutamate and nitric oxide (NO)-induced cytotoxicity, using isolated RGCs by a two-step panning method. Brain-derived neurotrophic factor (BDNF) was used as a positive control. EpoR mRNA was expressed in isolated RGCs, and EpoR protein was expressed on the RGCs in the normal and ischemic retinas. Epo had less potential to improve the survival of primary RGCs in serum-free medium than BDNF. In these cells, BDNF, but not Epo, downregulated the expression of Bim, a proapoptotic Bcl-2 family member that plays a key role in cytokine-mediated cell survival, suggesting a possible mechanism for this difference. When RGCs were cultured with glutamate or an NO-generating reagent, the survival of RGCs was compromised, and Bcl-2 expression was decreased in these cells. Both Epo and BDNF significantly reduced RGC death induced by glutamate and NO. In agreement with this, these factors reversed the Bcl-2 expression. These findings suggest that Epo may be a potent neuroprotective therapeutic agent for the treatment of ocular diseases that are characterized by RGC death.

Theme: Sensory systems
Topic: Retina and photoreceptors

Keywords: Primary isolated retinal ganglion cells; Glutamate; Nitric oxide; Bcl-2; Bim

1. Introduction

The death of retinal ganglion cells (RGCs), which results in the progressive loss of visual function, occurs in glaucoma and some ocular diseases [32,48]. Thus, the development of neuroprotective strategies that would prevent the death of RGCs is of critical importance.

Progress has been made in our understanding of the intracellular pathways that mediate stress-induced apoptosis in RGCs. For example, it is known that signals transmitted from NMDA (*N*-methyl-D-aspartate) and non-NMDA receptors induce cytotoxicity when they are overstimulated by excess amounts of glutamate [36,37,40,51], although glutamate is an important signaling molecule in physiological conditions as a neurotransmitter. Glutamate neurotoxicity is mediated, at least in part, by nitric oxide (NO) in retinal neurons [24,58]. Excess glutamate and NO were shown to be implicated in ischemic retinal degenerations, including glaucoma and diabetic retinopathy [19,22,28,35,43,47,48]. Antagonists of NMDA receptor were reported to show neuroprotective effects on glaucomatous optic neuropathy in

* Corresponding author. Fax: +81 82 257 5249.
E-mail address: hkmishi@hiroshima-u.ac.jp (H.K. Mishima).

0006-8993/$ - see front matter © 2005 Elsevier B.V. All rights reserved.
doi:10.1016/j.brainres.2005.05.037

experimental glaucoma models [19,28,43]. Moreover, NO synthase (NOS) levels were found to be elevated in the human glaucomatous optic nerve head [39]. In addition, glutamate and NO promote oxidative damage by reacting with superoxide anion to form the oxidant compound peroxynitrite [5,17,20], which triggers apoptotic cell death [48]. The oxidative stress has been shown to play an important role in the course of development of ischemic retinopathy [11,21]. Collectively, these findings suggest that the NMDA receptor and/or non-NMDA receptor-mediated pathways contribute to the pathogenesis of retinal diseases.

Neurotrophic factors may be a beneficial candidate for a neuroprotective agent. For example, brain-derived neurotrophic factor, (BDNF) not only supports survival of neurons including RGCs [8,14], but also has a neuroprotective function by inhibiting the cytotoxic action of glutamate and NO [30,31,55]. These effects of BDNF could be interpreted in part by regulating the expression or the function of specific members of the Bcl-2 superfamily, which includes both antiapoptotic and proapoptotic regulator proteins on mitochondrial membrane. In mammals, more than 5 member proteins are included in each group. Redundancy in each category of the Bcl-2 family has been partially explained by the death triggers-specific response of each family member. For example, Bim, a proapoptotic member, has been implicated in cytokine (neurotrophic factor)-dependent cell survival [2,42,49,60], while Bcl-2 or Bax has been suggested to be involved in cytotoxicity by glutamate and NO [56,57]. However, whether BDNF acts as a prosurvival factor through regulation of these family members is not clear.

Unfortunately, BDNF does not cross the blood–brain barrier (BBB) [61] and thus cannot be readily used therapeutically. Recently, the erythropoietin receptor (EpoR) was reported to be expressed in neurons [6,33,34]. In the hypoxic condition, EpoR expression in the cerebral cortex [44] was reported to be enhanced, suggesting a possible physiological role of the Epo/EpoR system in the central nervous system. Epo is required for the growth and development of erythroid progenitors [29] and is an established therapeutic agent to treat patients with renal anemia. Epo crosses the BBB [9], and the systemic administration of Epo has been reported to protect mouse photoreceptors from light-induced damage [18], rat retinal neurons from acute ischemic injury [23], and rat RGCs from axotomy-induced apoptosis in vivo [59]. Although these findings suggest that Epo might be useful in the treatment of retinal diseases, it is as yet unclear whether Epo protects isolated RGCs directly from glutamate- and NO-induced neurotoxicity, which is known to be implicated in ischemia.

We herein examined the ability of Epo to protect rat neonatal RGCs isolated by a two-step panning method [4] from the neurotoxic effects of glutamate and NO and compared its effects to those obtained with BDNF. Our results showed that Epo protected RGCs from the neurotoxic effects of glutamate and NO through the reversal of Bcl-2 expression.

2. Materials and methods

2.1. Isolation and culture of RGCs

All animals were treated in accordance with the ARVO Statement for the Use of Animals in Ophthalmic and Vision Research.

RGCs were isolated according to the previously described two-step panning method [4,25,26]. Briefly, 3-day-old Wistar rats were euthanized, and approximately 30 eyes were harvested for each experiment. The retinas that were separated from the enucleated eyeballs were incubated for 20 min in a solution containing 5 mg/ml papain in order to dissociate their cells, which was followed by a 5 min incubation with rabbit antimacrophage antibody (Inter-Cell Technologies, Hopewell, NJ). The cell suspensions were then incubated for 30 min on a 100-mm Petri dish coated with goat anti-rabbit IgG (H + L chain) antibody (Southern Biotechnology Associates, Birmingham, AL). Suspensions containing cells that did not adhere to the Petri dish were harvested and incubated for 1 h in a 100-mm dish coated with anti-Thy-1.1 antibody (from hybridoma T11D7e2; American Type Culture Collection, Rockville, MD). The cells that adhered to the dish were trypsinized off (0.125% trypsin for 10 min), after which they were incubated in 96-well plates that were coated with 0.1 mg/ml polyornithine (Sigma Chemical, St. Louis, MO) and 5 μg/ml laminin (Sigma Chemical, St. Louis, MO). Cells were cultured in serum-free medium [37], which was composed of Dulbecco's modified Eagle's medium supplemented with insulin (1.6×10^{-6} M), progesterone (4.0×10^{-8} M), selenite (6.0×10^{-8} M), transferrin (12.5×10^{-8} M), putrescine (2×10^{-4} M), hydrocortisone (1.0×10^{-7} M), cytidine-5′-diphosphocholine (5.2×10^{-6} M), cytidine-5′-diphosphoethanolamine (2.9×10^{-6} M), ciliary neurotrophic factor (CNTF: 40 ng/ml), and forskolin (1×10^{-5} M). Cells were incubated at 37 °C in a humidified atmosphere of 10% CO_2 and 90% air.

2.2. Retrograde transportation of tracer

The retrograde fluorescent tracer 1,1′-dioctadecyl-3,3,3′,3′-tetramethylindocarbocyanine perchlorate (DiI, Molecular Probes, Eugene, OR) was used as previously described [50]. Briefly, ten 1-day-old rats were anesthetized by hypothermia [41]. DiI, dissolved in dimethylformamide, was then injected subdurally into the superior colliculi. Three days later, RGCs from the 20 eyes of these animals were isolated, as described earlier [4,25,26], and were examined using fluorescent phase-contrast microscopy.

2.3. Immunohistochemical analysis of normal and ischemic retinas

Female Wistar rats weighing 250–300 g were used in this study. Rats were anesthetized with an intraperitoneal

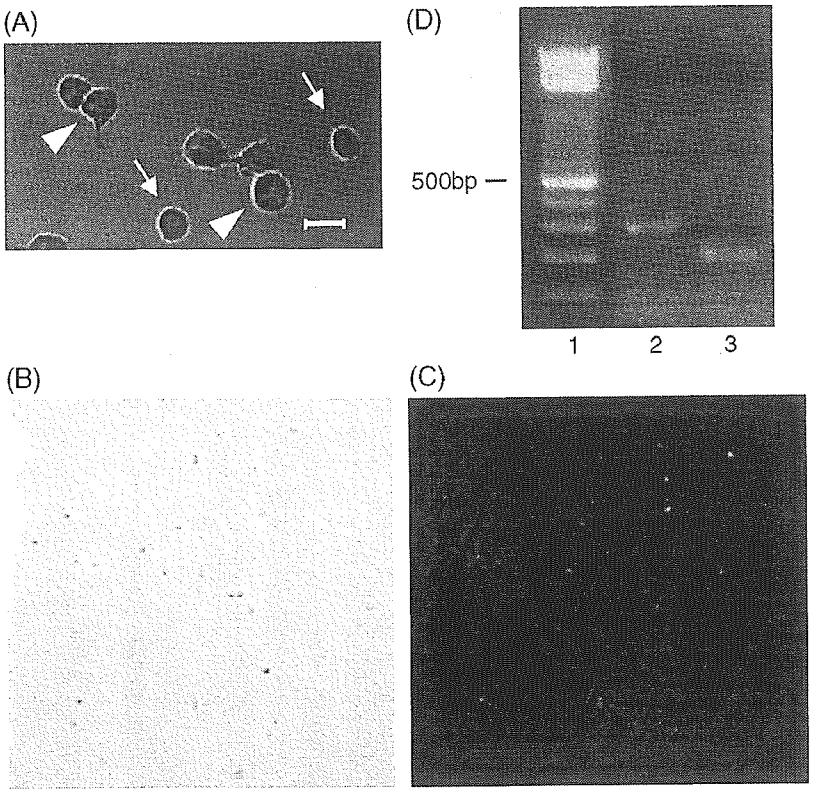

Fig. 1. Isolation and characterization of RGCs. (A) Phase-contrast image of isolated RGCs. Large cells (open arrowheads) and small cells (arrows) were seen. Scale bar, 10 μm. (B and C) Retrograde labeling images of RGCs. RGCs were isolated following injection of DiI into the superior colliculi. Cells were observed using phase-contrast microscopy (B), and DiI staining was visualized by fluorescent microscopy (C). (D) RT-PCR analysis revealed the expression of EpoR mRNA in the RGCs using a specific primer set (lane 3). Lane 1 = 100 bp DNA ladder as a marker. Lane 2 = β-actin used for normalization.

injection of pentobarbital (65 mg/kg). The anterior chamber of the right eye was cannulated with a 27-gauge infusion needle that was connected to a bottle containing sterile normal saline. Intraocular pressure was then raised to 120 mm Hg by elevating the saline reservoir to the appropriate height above the eye for 60 min. The animals' left eye was sham operated, and the reservoir to which it was connected was not elevated. These eyes served as non-ischemic controls.

For immunohistochemical analysis, eyes were enucleated 72 h after this operation and were fixed in 4% buffered paraformaldehyde overnight at 4 °C. The tissues were then transferred to phosphate buffer solution (PBS) containing sucrose, pH 7.4, at 4 °C. After removal of

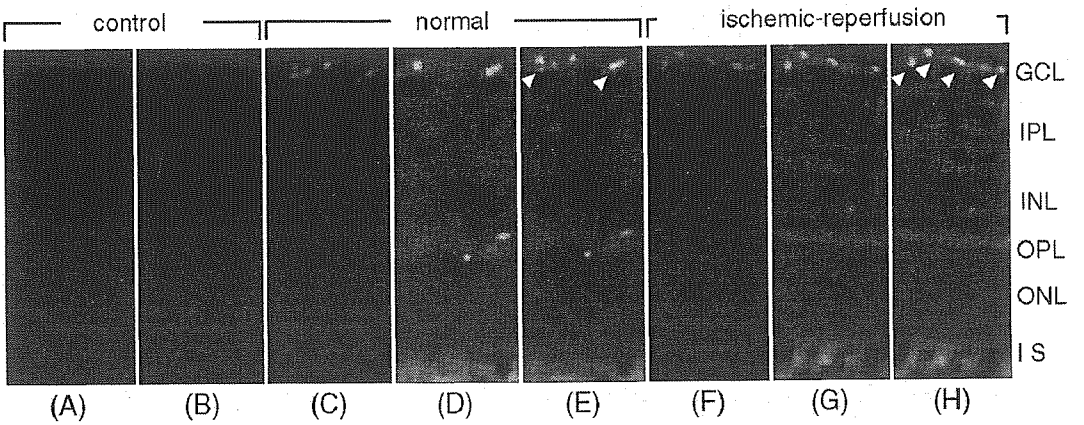

Fig. 2. Localization of EpoR in normal (A–E) and ischemic (F–H) retinas. (A, B) Negative control studies. Normal rat retina was incubated with rabbit control IgG and mouse control IgG followed by incubation with FITC-conjugated anti-rabbit IgG and Texas red-conjugated anti-mouse IgG. (C, F) RGCs were identified using a Thy-1.1 mouse monoclonal antibody and Texas red-conjugated anti-mouse IgG. (D, G) EpoR staining using an anti-EpoR rabbit polyclonal antibody and an FITC-conjugated anti-rabbit IgG. (E, H) Double staining for Thy-1.1 and EpoR (arrowheads). Slides were examined under the fluorescent microscopy. GCL, ganglion cell layer; IPL, inner plexiform layer; INL, inner nuclear layer; OPL, outer plexiform layer; ONL, outer nuclear layer; and IS, inner segment of photoreceptors.

the lenses, the eyecups were embedded in optimal cutting temperature (OCT) compound (Tissue Tek, Sakura, Tokyo, Japan). Cryosections (9 μm) were prepared at −80 °C. After they were dried, they were incubated in 10% horse serum in PBS to block nonspecific binding. After 3 washes in PBS, sections were incubated with anti-EpoR antibody (Santa Cruz Biotechnology, Santa Cruz, CA, rabbit polyclonal IgG, M-20, 0.7 μg/ml) overnight followed by fluorescein isothiocyanate (FITC)-conjugated goat anti-rabbit IgG (Vector, Burlingame, CA, goat polyclonal IgG, 7.5 μg/ml). Controls consisted of tissues that were treated with isotype control rabbit IgG (Wako pure chemicals, Osaka, JAPAN, 10 μg/ml). After being washed 3 times, the sections were incubated overnight with Thy-1.1 antibody (Pharmingen, San Diego, CA, mouse monoclonal IgG, clone OX-7, 10 μg/ml) or isotype control mouse IgG (BD Pharmingen, San Diego, CA, clone MOPC-31, 10 μg/ml). Next, they were washed and incubated with Texas red-conjugated anti-mouse IgG (H+L) (Vector, Burlingame, CA, horse polyclonal IgG, 15 μg/ml). The slides were then washed with PBS and examined with fluorescent microscopy.

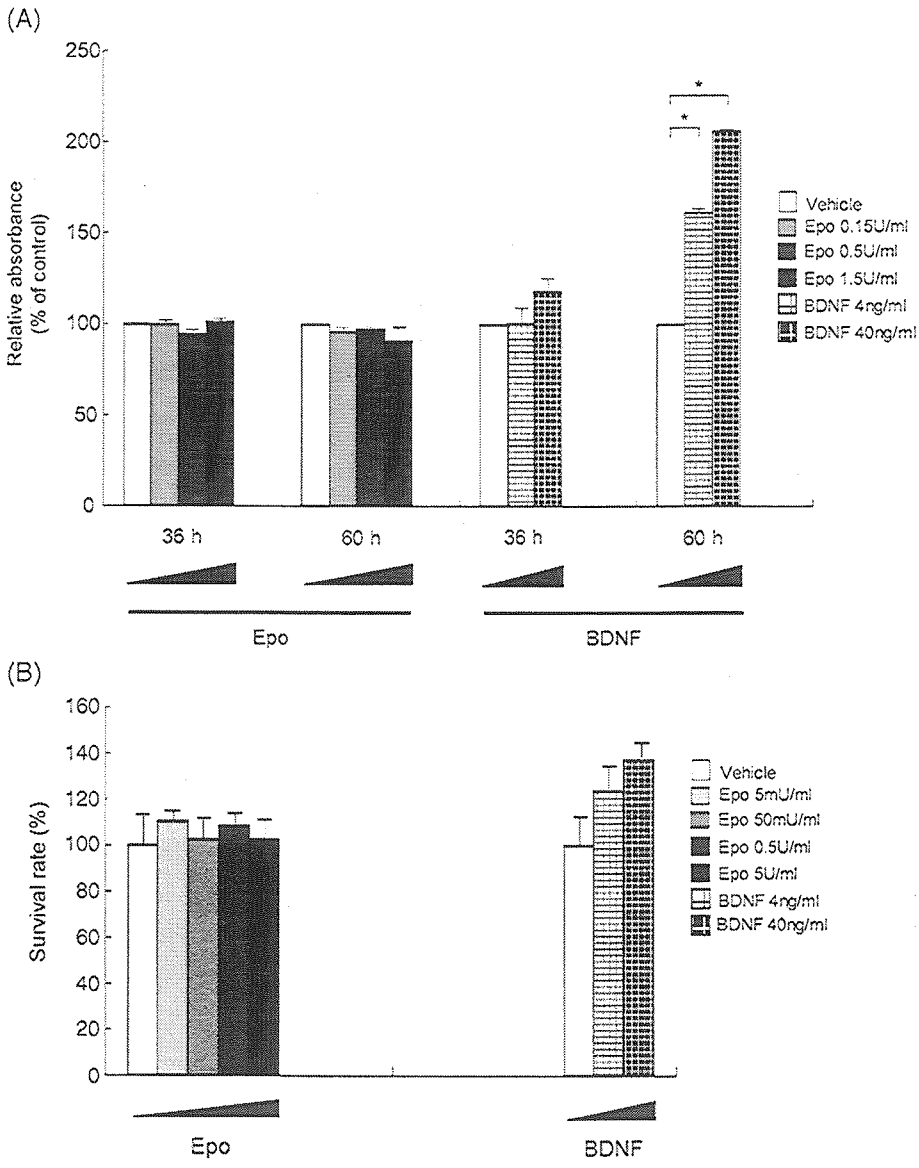

Fig. 3. Effects of Epo and BDNF on RGC survival. (A) Isolated RGCs were cultured in CNTF-containing medium (see Materials and methods) in the absence (open bars) or presence of Epo (0.15 U/ml — light gray bars; 0.5 U/ml — dark gray bars; 1.5 U/ml — black bars) (n = 5) or BDNF (4 ng/ml — white lattice bars; 40 ng/ml — black lattice bars) (n = 4) for 36 or 60 h, after which they were subjected to an XTT assay. The relative absorbance was calculated by each of XTT absorbance divided by that of control cultures in the absence of either Epo or BDNF. (B) Effects of Epo and BDNF on RGC survival in medium without CNTF and forskolin. Isolated RGCs were cultured in the absence (white bars) or presence of Epo (5 mU/ml — light gray bars; 50 mU/ml — gray bars; 0.5 U/ml — dark gray bars; 5 U/ml — black bars) (n = 4) or BDNF (4 ng/ml — white lattice bars; 40 ng/ml — black lattice bars) (n = 4) for 72 h, after which viability were evaluated by trypan blue exclusion. Each data point represents mean ± SEM. Asterisks denote a P value of <0.05 compared to the untreated control.

2.4. Detection of EpoR by reverse transcription-polymerase chain reaction (RT-PCR)

Total RNA was extracted using ISOGEN, according to the manufacturer's instructions (Nippongene, Toyama, Japan). cDNAs synthesized using a Superscript II kit (Invitrogen, Carlsbad, CA) were amplified with the following specific primer pairs: 5′-AAGATCTGGCCTGCATCCCAAG-3′; 5′-TCCCCAGCCTGAGTCACTCCCCAG-3′ for EpoR and 5′-TCATGAAGTGTGACGTTGACATCCGT-3′; 5′-CCTAGAAGCATTTGCGGTGCACGATG-3′ for β-actin, which resulted in PCR products of 197 bp and 285 bp in length, respectively. PCR products were cloned into a PCR™ II vector and sequenced using a genetic analyzer (310 Genetic Analyzer; Applied Biosystems, Foster City, CA).

2.5. Assessment of cell viability

Survival of RGCs that were incubated in the presence of glutamate, sodium nitroprusside (SNP), or *N*-omega-nitro-L-arginine methyl ester (L-NAME) in the presence or absence of Epo or BDNF was estimated by determining the activity of their mitochondrial dehydrogenases (sodium3′[1-(phenylaminocarbonyl)-3,4-tetrazolium]-bis (4-methoxy-6-nitro) benzene sulfonic acid hydrate) using the XTT assay according to the manufacturer's directions (XTT kit II; Roche Diagnostics GmbH, Mannheim, Germany). Briefly, RGCs were cultured in 96-well plates, and the 1 mg/ml XTT labeling solution was added to each well in the culture medium, after which the plate was incubated for 3 h in a humidified atmosphere. The absorbance of each sample was measured at a wavelength of 450 and 595 nm (reference wavelength). The relative absorbance was calculated by dividing the XTT absorbance of cells by the absorbance of cells cultured without the test substances. Cell viability of RGCs that were incubated in the absence of CNTF and forskolin was assessed by bright-field microscopy using a 0.4% trypan blue exclusion method. The mean survival was determined by counting four randomly selected fields per well.

2.6. Real-time quantitative RT-PCR

Total RNA and cDNA were prepared as described above. The sequences of the primers were 5′-(GTGGTGGAGGAACTCTTCAGGGATG)-3′; 5′ (GGTCTTCAGAGACAGCCAGGAGAAATC)-3′ for Bcl-2, 5′-(GTAGTGAATGAACTCTTTCGGGATGG)-3′; 5′-(ACCAGCCACAGTCATGCCCGTCAGG)-3′ for Bcl-xL, 5′-(AGTGGGTATTTCTCTTTTGACACAG)-3′; 5′-(TCAGTGCCTTCTCCAGACCAGACG)-3′ for Bim, 5′-(AATATGGAGCTGCAGAGGATGATTG)-3′; 5′-(GCACTTTAGTGCACAGGGCCTTGAG)-3′ for Bax. Real-time RT-PCR reactions were performed using SYBER-Green One-Step RT-PCR Master Mix reagent kit and Prism 7700 (Applied Biosystems, Foster City, CA) in a total volume of 50 μl of reaction mixture. Each sample was normalized to the content of β-actin transcript.

2.7. Statistical analysis

Statistical significance between the various experimental groups was determined by one-way analysis of variance (ANOVA) followed by a Tukey–Kramer post hoc test. Significant differences were defined by a P value of <0.05. All data are expressed as the mean ± SEM.

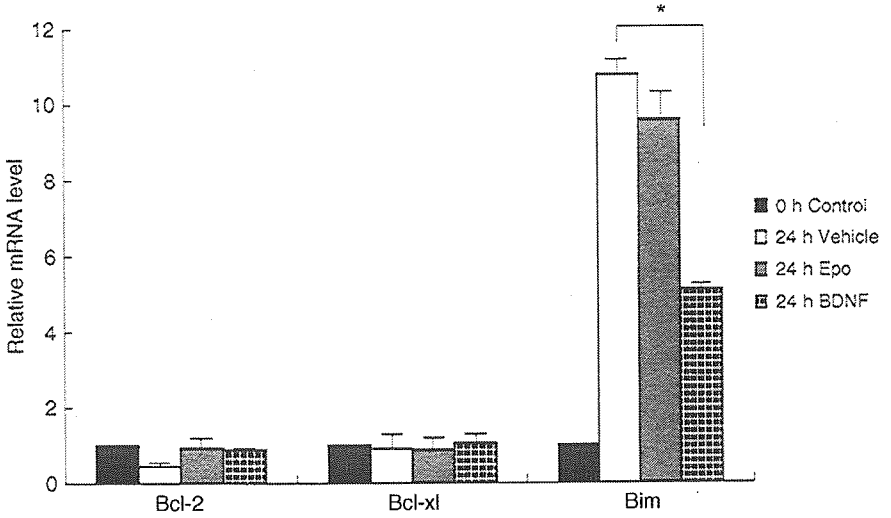

Fig. 4. Expression of Bcl-2, Bcl-x_L, and Bim in RGCs. Cells were cultured in the presence or absence of Epo (8.25 U/ml) or BDNF (100 ng/ml) for 24 h. Real-time quantitative RT-PCR was then carried out, and the numbers of cycles required to produce a detectable product were measured and used to calculate fold-differences in starting mRNA level for each sample using β-actin as the internal control. Levels of mRNA in cells cultured in the absence of Epo or BDNF (open bars) or in the presence of Epo (dark gray bars) or BDNF (black lattices bars) relative to cells collected immediately after isolation (control, black bars) are shown. Each data point represents mean ± SEM. $n = 3$. Asterisks denote a P value of <0.05.

3. Results

3.1. Expression of EpoR in primary cultured RGCs

RGCs were isolated from neonatal rats in the two-step panning method and cultured in serum-free medium. The average yield of isolated RGCs was 1.4 ± 0.2% of dissociated retinal cells, which was similar to our previously reported data [45]. Two types of RGCs were identified in our cell cultures: large cells (10–12 μm in diameter) that were somewhat spindle shaped, most of which had a comparatively long process (Fig. 1A, open arrowheads), and small round cells (6–8 μm in diameter), most of which had a thick, short process (arrows) [25]. To evaluate the purity of the RGC population, we employed DiI, which is incorporated by RGCs in a retrograde manner, when injected into the superior colliculi. More than 90% of the isolated cells were positive for DiI (Figs. 1B,C), indicating that the vast majority of isolated cells were RGC. To examine EpoR gene expression, RT-PCR was performed using total RNA extracted from the isolated RGCs. The expected band of appropriate size was detected (Fig. 1D, lane 3), which was confirmed to be rat EpoR cDNA by sequence analysis.

We confirmed the expression of EpoR in RGCs in the rat retina immunohistochemically. EpoR was mainly detected in the outer plexiform layer (OPL), the inner segment of photoreceptors (IS), and the ganglion cell layer (GCL) of the normal rat retina. Weak staining was also detected in the inner plexiform layer (IPL) (Figs. 2B,D). Cells expressing EpoR in the GCL overlapped with those labeled with the Thy-1.1 antibody (Figs. 2A,C,E). We repeated the experi-

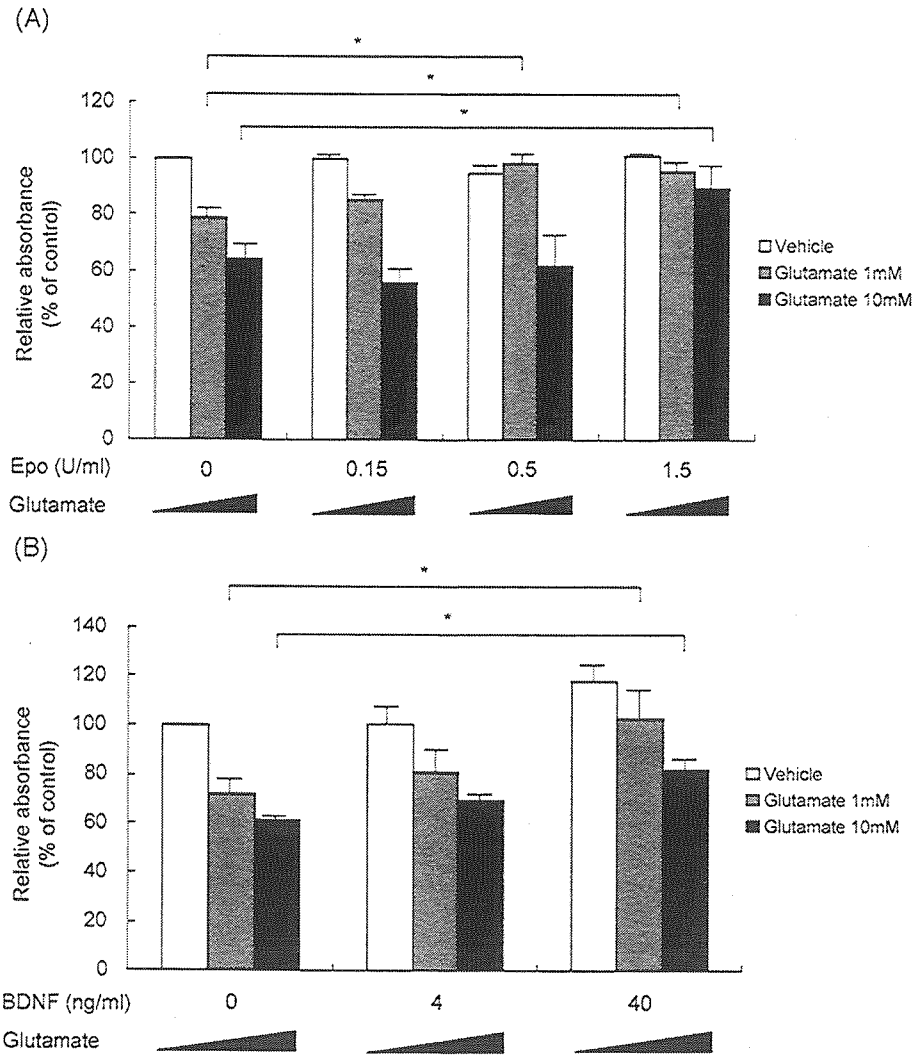

Fig. 5. Epo and BDNF protected RGCs from the cytotoxic effects of high concentrations of glutamate. RGCs were cultured in the presence or absence of Epo (0.15, 0.5, 1.5 U/ml) (n = 5) (A) or BDNF (4, 40 ng/ml) (n = 4) (B) for 12 h, after which they were cultured for additional 24 h with or without glutamate at a final concentration of 1 or 10 mM. The cells were then subjected to an XTT assay. The relative absorbance was calculated by each of XTT absorbance divided by that of control cultures in the absence of Epo, BDNF, or glutamate. Each data point represents mean ± SEM. Asterisks denote a P value of <0.05, compared to the untreated control.

ments using the rat retina in ischemic conditions induced by elevated intraocular pressure. Similar results were obtained (Figs. 2F,G,H), indicating that EpoR was expressed in RGCs in the normal and ischemic retinas.

3.2. Function of Epo to support RGC survival

We initially tested if Epo can support RGC survival. Isolated RGCs were cultured in serum-free medium in the presence or absence of Epo or BDNF, after which the XTT assay was performed to evaluate their survival. The presence of different concentrations of Epo (0.15–1.5 U/ml) for either 36 or 60 h did not improve the survival (Fig. 3A). In contrast, RGC survival improved when they were cultured for 60 h in the presence of BDNF (4 and 40 ng/ml), although this effect was not evident when RGCs were cultured with BDNF for 36 h (Fig. 3A). These data suggest that Epo has less potential to improve the RGC survival in serum-free medium than BDNF.

Culture medium used in the above experiments contains CNTF, which is known to be a survival factor. Thus, we repeated the experiments using medium without CNTF and forskolin. The presence of different concentrations of Epo (0.005–5 U/ml) for 72 h did not improve the survival of RGCs (Fig. 3B). As expected, BDNF (4 and 40 ng/ml) supported the survival or RGCs.

These findings could be explained by different effects of these cytokines on the expression of Bcl-2 superfamily members such as Bcl-2, Bcl-x_L, or Bim. Real-time quantitative RT-PCR revealed that the mRNA levels of Bim, a proapoptotic relative of Bcl-2 family member, was markedly upregulated in RGCs cultured in serum-free medium for 24 h, while the expression levels of Bcl-2 and Bcl-x_L did not change significantly (Fig. 4). In the presence of Epo (8.25 U/ml), the induction of Bim was only marginally suppressed. By contrast, BDNF (100 ng/ml) reduced its expression of Bim significantly (Fig. 4), suggesting a possible involvement of Bim in the mecha-

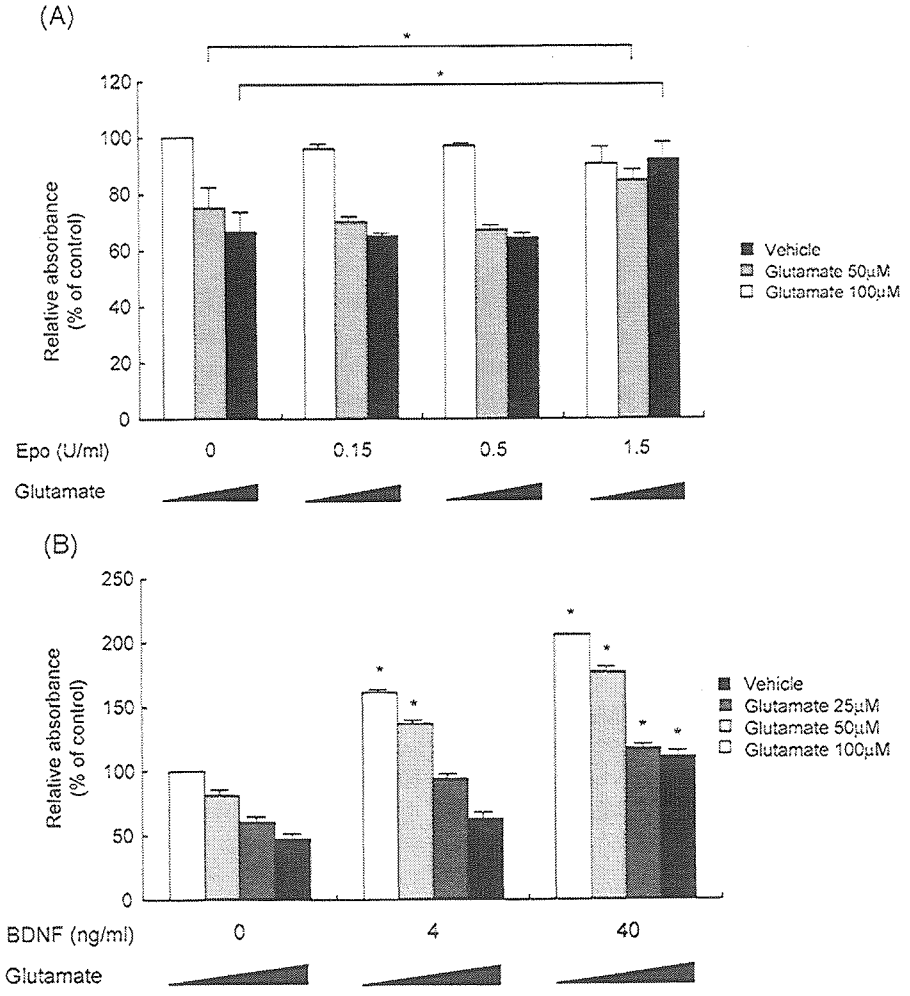

Fig. 6. Epo and BDNF protected RGCs from the cytotoxic effects of low concentrations of glutamate. Isolated RGCs were cultured in the presence or absence of Epo (0.15, 0.5, 1.5 U/ml) ($n = 4$) (A) or BDNF (4, 40 ng/ml) ($n = 4$) (B) for 12 h, after which they were cultured for an additional 48 h with or without glutamate at a final concentration of 25, 50, or 100 μM. The cells were then subjected to an XTT assay. The relative absorbance was calculated by each instance of XTT absorbance divided by that of control cultures in the absence of Epo, BDNF, or glutamate. Each data point represents mean ± SEM. Asterisks denote a P value of <0.05 compared to the untreated control.

nism through which BDNF improves the survival of RGCs (Fig. 3).

3.3. Neuroprotective effect of Epo on RGCs from glutamate toxicity

To examine glutamate-induced cytotoxicity, we cultured isolated RGCs in different concentrations of glutamate, after which an XTT assay was performed. Glutamate-induced cytotoxicity at the concentrations of ≤100 μM was not evident until after 48 h, while RGCs were damaged within 24 h after the addition of high concentrations of glutamate (≥1 mM). Thus, we cultured RGCs for 48 h with glutamate at low concentrations (≤100 μM) or for 24 h at high concentrations (≥1 mM). The relative absorbance in RGC cultures was reduced by glutamate in a concentration-dependent manner (Figs. 5 and 6), which confirmed earlier reports [26,40]. Pretreatment with Epo for 12 h at a concentration of 0.5 U/ml significantly prevented the toxic effects of 1 mM glutamate (Fig. 5A). A high concentration of Epo (1.5 U/ml) also prevented glutamate-induced toxicity at each concentration we tested (Figs. 5A and 6A). As expected from previous reports [27,30], BDNF had a dose-dependent protective effect on glutamate-induced cytotoxicity (Figs. 5B and 6B). The use of Epo and BDNF in combination did not result in additional or synergic protection (data not shown).

3.4. Neuroprotection of RGCs from nitric oxide toxicity by Epo

The above results showed that Epo protected RGCs from glutamate-induced cytotoxicity. To probe the mechanism of the neuroprotective effect of Epo, we examined whether Epo could inhibit cell death induced by NO because NO was recently shown to be a downstream mediator of glutamate-induced cytotoxicity [1]. In accordance with this report, a general NOS inhibitor, L-NAME, partially reversed glutamate toxicity in RGCs (Fig. 7A). To determine whether Epo protects RGCs from NO-induced toxicity, RGCs were pretreated with or without Epo for 12 h, after which they were treated with different concentrations of an NO-generating agent SNP for 6 h. RGCs succumbed to SNP in a dose-dependent fashion, and Epo (1.5 U/ml) prevented the toxicity induced by 100 and 500 μM concentrations of SNP (Fig. 7B). BDNF (40 ng/ml) also inhibited SNP toxicity at 100 and 500 μM. These data suggest that Epo protects RGCs from glutamate-induced cytotoxicity, in part, by preventing NO-induced toxicity.

To investigate the mechanism of neuroprotective effect of Epo from NO-induced toxicity, we examined whether Epo could reverse the expression of Bcl-2 superfamily members. Real-time quantitative RT-PCR revealed that the mRNA levels of Bcl-2 was markedly downregulated in RGCs cultured with SNP (500 μM) for 6 h in the absence of Epo or BDNF (Fig. 7C). In the presence of Epo or BDNF, the expression levels of Bcl-2 were significantly reversed in a dose-dependent manner. Similar results were obtained in Bcl-x_L expression, although they were not statistically significant, while little difference was observed in the expression levels of Bim and Bax. These findings suggest a possible involvement of Bcl-2 in the mechanism through which Epo and BDNF protect RGCs from NO-induced toxicity.

4. Discussion

We herein demonstrated that isolated primary cultured RGCs expressed EpoR mRNA (Fig. 1D), as RGCs in the normal and ischemic retinas expressed EpoR protein (Fig. 2). To test whether Epo would be beneficial for the treatment of ocular diseases, we studied its biological effects on isolated RGCs. In contrast to BDNF, which showed prominent potential to support cell survival of RGCs, Epo had a little potential to support the survival of RGCs in serum-free medium in our experimental system. Nevertheless, Epo protected RGCs from glutamate-induced cytotoxicity (Figs. 5A and 6A). This effect likely occurred through its potential to prevent NO-induced cytotoxicity by the reversal of Bcl-2 expression, at least in part (Fig. 8).

EpoR is expressed in non-ischemic cerebral neurons [34], and its expression was reported to be upregulated by hypoxia/ischemia [12,44]. In the rat retina, under the normal or ischemic condition, we detected EpoR expression in the GCL, IPL, OPL, and IS (Fig. 2), confirming an earlier report [7]. Weishaupt et al. also reported that EpoR expressed in the GCL, although they found its expression in the inner nuclear layer (INL) and outer nuclear layer (ONL) of the normal rat retina and did not find in the IPL and OPL [59]. However, Grimm et al. did not detect EpoR expression in the GCL of the normal mouse retina [18]. Although the

Fig. 7. Epo and BDNF protected RGCs from NO-induced toxicity. (A) RGCs were cultured in serum-free medium for 24 h in the presence of glutamate (1 mM) with or without pretreatment with L-NAME (100 μM) for 30 min. (B) Isolated RGCs were cultured in the presence or absence of Epo (1.5 U/ml) or BDNF (40 ng/ml) for 12 h, after which the cells were cultured for additional 6 h in the presence or absence of SNP at a final concentration of 10, 100, or 500 μM. The cells were then subjected to an XTT assay. The relative absorbance was calculated by each of XTT absorbance divided by that of control cultures in the absence of Epo, BDNF, or SNP. (C) Expression of Bcl-2, Bcl-x_L, Bim, and Bax in RGCs. Cells were cultured in the presence or absence of Epo (1.5, 8.25 U/ml) or BDNF (40, 100 ng/ml) for 3 h, after which the cells were cultured for additional 6 h in the presence or absence of SNP (500 μM). Real-time quantitative RT-PCR was then carried out, and the numbers of cycles required to produce a detectable product were measured and used to calculate fold-differences in starting mRNA level for each sample using β-actin as the internal control. Levels of each mRNA in cells cultured with SNP in the absence of Epo or BDNF (light gray bars) or in the presence of Epo (1.5 U/ml — dark gray bars; 8.25 U/ml — black bars) or BDNF (40 ng/ml — white lattice bars; 100 ng/ml — dark lattice bars) relative to untreated cells (control, open bars) are shown. Each data point represents mean ± SEM. $n = 4$. Asterisks denote a P value of <0.05.

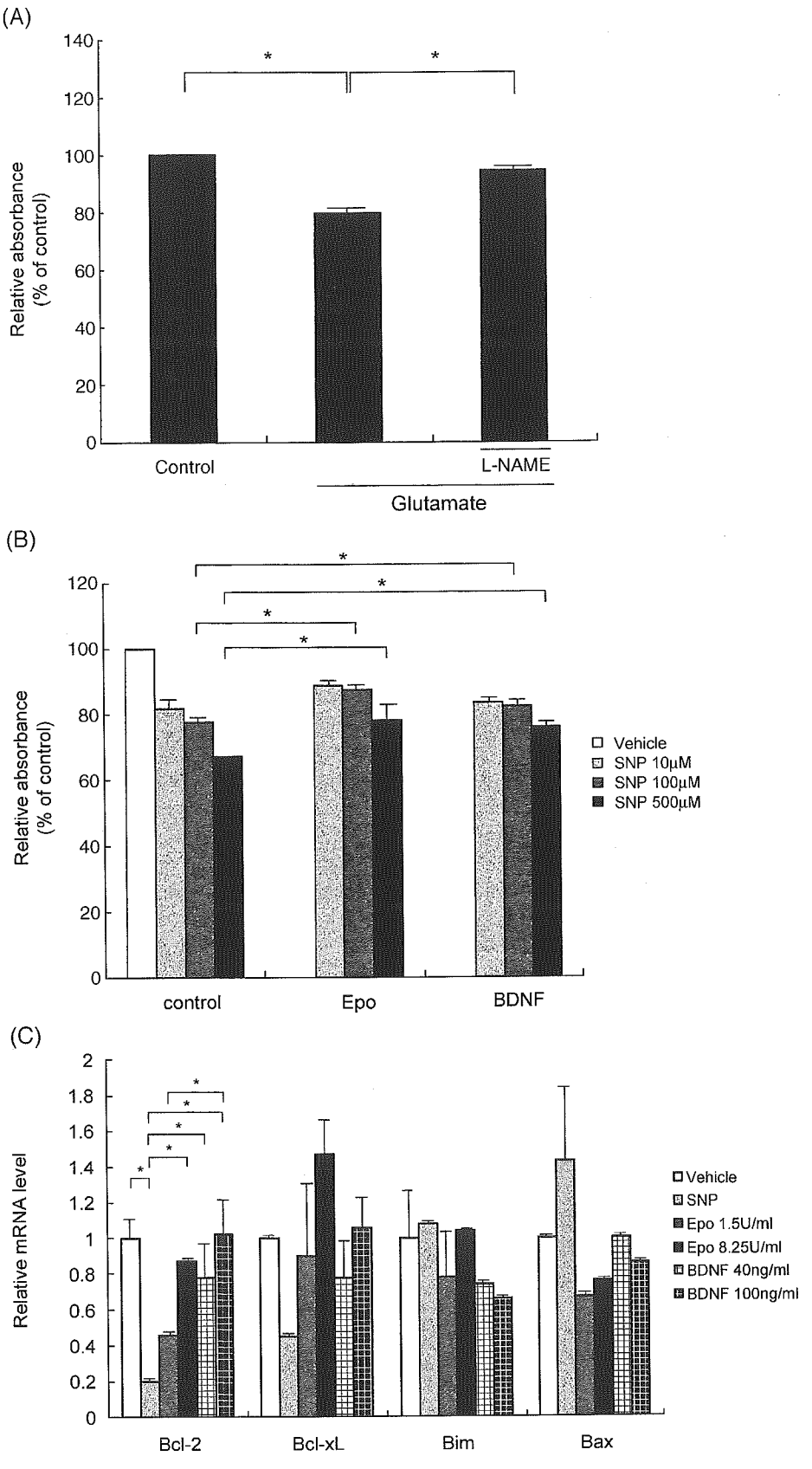
(A)
Relative absorbance (% of control)
140
120
100
80
60
40
20
0
*
*
Control
L-NAME
Glutamate
(B)
Relative absorbance (% of control)
120
100
80
60
40
20
0
*
*
*
*
control
Epo
BDNF
Vehicle
SNP 10μM
SNP 100μM
SNP 500μM
(C)
Relative mRNA level
2
1.8
1.6
1.4
1.2
1
0.8
0.6
0.4
0.2
0
*
*
*
*
*
Bcl-2
Bcl-xL
Bim
Bax
Vehicle
SNP
Epo 1.5U/ml
Epo 8.25U/ml
BDNF 40ng/ml
BDNF 100ng/ml

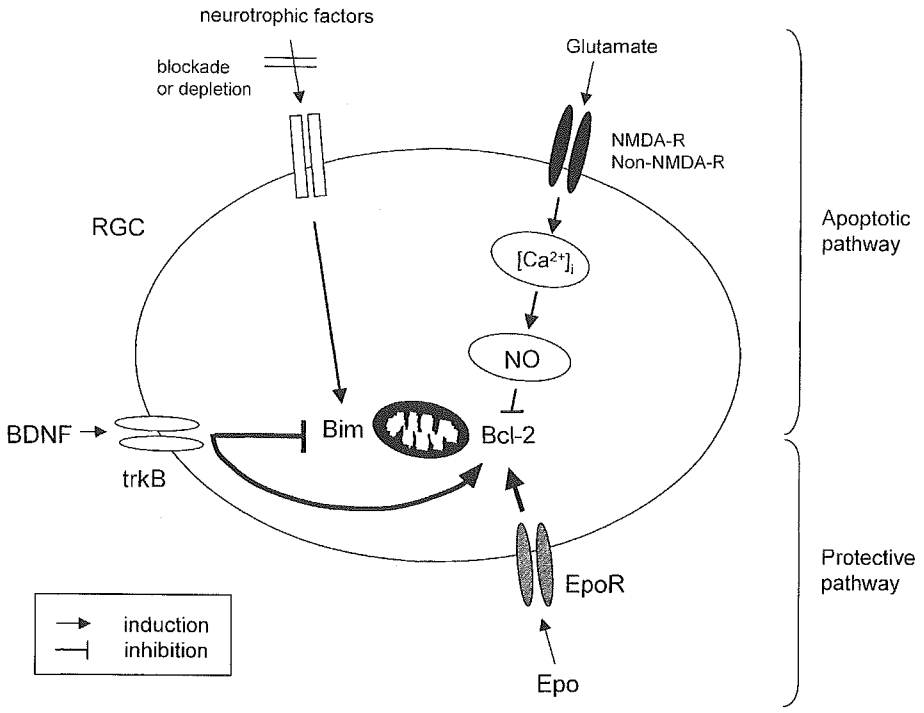

Fig. 8. Schematic representation of the signaling pathways that mediate the regulation of apoptosis of RGCs. Bim is induced in RGCs cultured in serum-free medium without neurotrophic factors. BDNF, not Epo, reverses the induction of Bim. NMDA and non-NMDA-receptor-mediated pathways, which downregulate Bcl-2 through NOS activation, at least in part. Epo as well as BDNF recover Bcl-2 expression. The lines in bold face represent the signaling pathways that were found to be regulated by Epo and BDNF in this study.

reason for these discrepancies is unclear, we believe that rat RGCs under the normal or ischemic condition express EpoR because we observed that expression of EpoR and Thy-1.1 overlapped (Figs. 2E,H). This is also supported by detection of EpoR mRNA in isolated RGCs (Fig. 1D).

Whether Epo can support survival of neurons in serum-free medium has been a disputed question. Tabira et al. showed that Epo promoted survival of cholinergic neurons [54], and their findings were supported in reports by others on primary motoneurons, neuronally differentiated embryonal carcinoma P19 cells, and primary cultured RGCs [53,59]. However, findings in other reports did not provide clear evidence that Epo supports survival of hippocampal [34] and cerebrocortical neurons [16,52]. Our results suggested that Epo has less potential to improve survival of primary RGCs in serum-free medium than BDNF (Fig. 3). This is consistent with our findings that, unlike BDNF, Epo was unable to attenuate Bim mRNA expression (Fig. 4) because Bim was recently established to be a key factor in cytokine (neurotrophic factor)-dependent cell survival [2,42,49,60]. Cytokines and neurotrophic factors downregulate Bim expression transcriptionally and/or posttranscriptionally in a cell lineage-specific manner. Indeed, nerve growth factor (NGF) and BDNF inhibit Bim expression in rat sympathetic neurons or human neuroblastoma cells [60,62]. In the case of RGCs, Bim mRNA expression was highly induced in the absence of neurotrophic factors (Fig. 4), suggesting that downregulation of Bim mRNA is critical for maintaining cell viability (Fig. 8). This hypothesis is consistent with the result in a recent paper reporting that Bim mRNA level is induced in RGCs undergoing apoptosis by transection of the optic nerve [38].

BDNF likely protects RGCs from glutamate-mediated cell death by two mechanisms. One is by supporting cell survival (Fig. 3) that inhibits apoptosis by downregulating Bim (Figs. 4 and 8). This mechanism seems to be dominant when cells were cultured for a longer period (60 h) at low concentrations of glutamate (Fig. 6B). The other is through its neuroprotective function by downregulating NMDA or non-NMDA-receptor-mediated pathways (Fig. 8), which mediate calcium influx and NOS activity [15,51,58]. This effect appeared to be evident when cells were cultured for a shorter period (36 h) at high glutamate concentrations (Fig. 5B) because BDNF (40 ng/ml) reversed glutamate-induced toxicity when no significant improvement of cell survival was observed in glutamate-free medium.

Whereas Epo had a little potential to improve RGCs in serum-free medium (Fig. 3), Epo protects RGCs from glutamate- and NO-mediated cell death (Figs. 5–7). Previous reports also demonstrated that Epo protects hippocampal and cerebral cortical neurons from NO [10,13,46]. NO induces apoptosis in neurons after alteration of the expression levels of specific members of the Bcl-2 superfamily. For example, NO downregulates Bcl-2 and upregulates Bax in cortical neurons and hippocampal neuronal cells [56,57]. In addition, NO induced by hypoxia increases Bax gene expression in cerebral neurons [63].

Our data demonstrated that NO downregulates Bcl-2 expression in isolated RGC cultures, and either Epo or BDNF reversed Bcl-2 mRNA levels in a dose-dependent manner (Fig. 7C). These findings support a possible mechanism that Epo and BDNF protect RGCs from NO-induced toxicity (Fig. 8), although upstream pathways which upregulate Bcl-2 by these two neurotrophic factors remain to be established.

Collectively, these data suggest that, while Epo cannot substitute for BDNF in promoting RGC survival in serum-free medium, it could still be useful in protecting RGCs from glutamate- and NO-induced toxicity, which has been implicated in glaucoma and ocular diseases caused by hypoxia and ischemia, such as diabetic retinopathy [3,19,22,28,39,47,48]. Thus, Epo may be a beneficial candidate for a neuroprotective agent for treating these ocular diseases.

Acknowledgments

This study was supported by a grant-in-aid (16791049) from the Ministry of Education, Culture, Sports, Science and Technology of Japan and supported by a grant (H15-Sensor-003) from the Ministry of Health, Labor and Welfare of Japan.

References

[1] K. Adachi, S. Kashii, H. Masai, M. Ueda, C. Morizane, K. Kaneda, T. Kume, A. Akaike, Y. Honda, Mechanism of the pathogenesis of glutamate neurotoxicity in retinal ischemia, Graefes Arch. Clin. Exp. Ophthalmol. 236 (1998) 766–774.

[2] T. Akiyama, P. Bouillet, T. Miyazaki, Y. Kadono, H. Chikuda, U.I. Chung, A. Fukuda, A. Hikita, H. Seto, T. Okada, T. Inaba, A. Sanjay, R. Baron, Regulation of osteoclast apoptosis by ubiquitination of proapoptotic BH3-only Bcl-2 family member Bim, EMBO J. 22 (2003) 6653–6664.

[3] J. Ambati, K.V. Chalam, D.K. Chawla, C.T. D'Angio, E.G. Guillet, S.J. Rose, R.E. Vanderlinde, B.K. Ambati, Elevated gamma-amino-butyric acid, glutamate, and vascular endothelial growth factor levels in the vitreous of patients with proliferative diabetic retinopathy, Arch. Ophthalmol. 115 (1997) 1161–1166.

[4] B.A. Barres, B.E. Silverstein, D.P. Corey, L.L. Chun, Immunological, morphological, and electrophysiological variation among retinal ganglion cells purified by panning, Neuron 1 (1988) 791–803.

[5] J.S. Beckman, T.W. Beckman, J. Chen, P.A. Marshall, B.A. Freeman, Apparent hydroxyl radical production by peroxynitrite: implications for endothelial injury from nitric oxide and superoxide, Proc. Natl. Acad. Sci. U. S. A. 87 (1990) 1620–1624.

[6] M. Bernaudin, H.H. Marti, S. Roussel, D. Divoux, A. Nouvelot, E.T. MacKenzie, E. Petit, A potential role for erythropoietin in focal permanent cerebral ischemia in mice, J. Cereb. Blood Flow Metab. 19 (1999) 643–651.

[7] S. Bocker-Meffert, P. Rosenstiel, C. Rohl, N. Warneke, J. Held-Feindt, J. Sievers, R. Lucius, Erythropoietin and VEGF promote neural outgrowth from retinal explants in postnatal rats, Invest. Ophthalmol. Visual Sci. 43 (2002) 2021–2026.

[8] D. Bonnet, M. Garcia, E. Vecino, J.G. Lorentz, J. Sahel, D. Hicks, Brain-derived neurotrophic factor signalling in adult pig retinal ganglion cell neurite regeneration in vitro, Brain Res. 1007 (2004) 142–151.

[9] M.L. Brines, P. Ghezzi, S. Keenan, D. Agnello, N.C. de Lanerolle, C. Cerami, L.M. Itri, A. Cerami, Erythropoietin crosses the blood–brain barrier to protect against experimental brain injury, Proc. Natl. Acad. Sci. U. S. A. 97 (2000) 10526–10531.

[10] G. Calapai, M.C. Marciano, F. Corica, A. Allegra, A. Parisi, N. Frisina, A.P. Caputi, M. Buemi, Erythropoietin protects against brain ischemic injury by inhibition of nitric oxide formation, Eur. J. Pharmacol. 401 (2000) 349–356.

[11] A. Ceriello, New insights on oxidative stress and diabetic complications may lead to a "causal" antioxidant therapy, Diabetes Care 26 (2003) 1589–1596.

[12] K. Chin, X. Yu, B. Beleslin-Cokic, C. Liu, K. Shen, H.W. Mohrenweiser, C.T. Noguchi, Production and processing of erythropoietin receptor transcripts in brain, Brain Res. Mol. Brain Res. 81 (2000) 29–42.

[13] Z.Z. Chong, S.H. Lin, J.Q. Kang, K. Maiese, Erythropoietin prevents early and late neuronal demise through modulation of Akt1 and induction of caspase 1, 3, and 8, J. Neurosci. Res. 71 (2003) 659–669.

[14] S. Cohen-Cory, S.E. Fraser, Effects of brain-derived neurotrophic factor on optic axon branching and remodelling in vivo, Nature 378 (1995) 192–196.

[15] T.M. Dawson, S.H. Snyder, Gases as biological messengers: nitric oxide and carbon monoxide in the brain, J. Neurosci. 14 (1994) 5147–5159.

[16] M. Digicaylioglu, S.A. Lipton, Erythropoietin-mediated neuroprotection involves cross-talk between Jak2 and NF-kappaB signalling cascades, Nature 412 (2001) 641–647.

[17] A.B. El-Remessy, I.E. Khalil, S. Matragoon, G. Abou-Mohamed, N.J. Tsai, P. Roon, R.B. Caldwell, R.W. Caldwell, K. Green, G.I. Liou, Neuroprotective effect of (-)Delta9-tetrahydrocannabinol and cannabidiol in *N*-methyl-D-aspartate-induced retinal neurotoxicity: involvement of peroxynitrite, Am. J. Pathol. 163 (2003) 1997–2008.

[18] C. Grimm, A. Wenzel, M. Groszer, H. Mayser, M. Seeliger, M. Samardzija, C. Bauer, M. Gassmann, C.E. Reme, HIF-1-induced erythropoietin in the hypoxic retina protects against light-induced retinal degeneration, Nat. Med. 8 (2002) 718–724.

[19] Z. Gu, T. Yamamoto, C. Kawase, M. Matsubara, K. Kawase, A. Sawada, Y. Kitazawa, Neuroprotective effect of *N*-methyl-D-aspartate receptor antagonists in an experimental glaucoma model in the rat, Nippon Ganka Gakkai Zasshi 104 (2000) 11–16.

[20] P.G. Gunasekar, A.G. Kanthasamy, J.L. Borowitz, G.E. Isom, NMDA receptor activation produces concurrent generation of nitric oxide and reactive oxygen species: implication for cell death, J. Neurochem. 65 (1995) 2016–2021.

[21] P. Hardy, I. Dumont, M. Bhattacharya, X. Hou, P. Lachapelle, D.R. Varma, S. Chemtob, Oxidants, nitric oxide and prostanoids in the developing ocular vasculature: a basis for ischemic retinopathy, Cardiovasc. Res. 47 (2000) 489–509.

[22] W.K. Ju, K.Y. Kim, S.J. Park, D.K. Park, C.B. Park, S.J. Oh, J.W. Chung, M.H. Chun, Nitric oxide is involved in sustained and delayed cell death of rat retina following transient ischemia, Brain Res. 881 (2000) 231–236.

[23] A.K. Junk, A. Mammis, S.I. Savitz, M. Singh, S. Roth, S. Malhotra, P.S. Rosenbaum, A. Cerami, M. Brines, D.M. Rosenbaum, Erythropoietin administration protects retinal neurons from acute ischemia–reperfusion injury, Proc. Natl. Acad. Sci. U. S. A. 99 (2002) 10659–10664.

[24] S. Kashii, M. Mandai, M. Kikuchi, Y. Honda, Y. Tamura, K. Kaneda, A. Akaike, Dual actions of nitric oxide in *N*-methyl-D-aspartate receptor-mediated neurotoxicity in cultured retinal neurons, Brain Res. 711 (1996) 93–101.

[25] F. Kashiwagi, K. Kashiwagi, Y. Iizuka, S. Tsukahara, Effects of brain-derived neurotrophic factor and neurotrophin-4 on isolated cultured retinal ganglion cells: evaluation by flow cytometry, Invest. Ophthalmol. Visual Sci. 41 (2000) 2373–2377.

[26] K. Kashiwagi, Y. Iizuka, M. Araie, Y. Suzuki, S. Tsukahara, Effects of retinal glial cells on isolated rat retinal ganglion cells, Invest. Ophthalmol. Visual Sci. 42 (2001) 2686–2694.
[27] N. Kido, H. Tanihara, M. Honjo, M. Inatani, T. Tatsuno, C. Nakayama, Y. Honda, Neuroprotective effects of brain-derived neurotrophic factor in eyes with NMDA-induced neuronal death, Brain Res. 884 (1–2) (2000) 59–67.
[28] M. Kikuchi, L. Tenneti, S.A. Lipton, Role of p38 mitogen-activated protein kinase in axotomy-induced apoptosis of rat retinal ganglion cells, J. Neurosci. 20 (2000) 5037–5044.
[29] M.J. Koury, M.C. Bondurant, Erythropoietin retards DNA breakdown and prevents programmed death in erythroid progenitor cells, Science 248 (1990) 378–381.
[30] T. Kume, H. Kouchiyama, S. Kaneko, T. Maeda, S. Kaneko, A. Akaike, S. Shimohama, T. Kihara, J. Kimura, K. Wada, S. Koizumi, BDNF prevents NO mediated glutamate cytotoxicity in cultured cortical neurons, Brain Res. 756 (1997) 200–204.
[31] T. Kume, H. Nishikawa, H. Tomioka, H. Katsuki, A. Akaike, S. Kaneko, T. Maeda, T. Kihara, S. Shimohama, p75-mediated neuroprotection by NGF against glutamate cytotoxicity in cortical cultures, Brain Res. 852 (2000) 279–289.
[32] L.A. Levin, Retinal ganglion cells and neuroprotection for glaucoma, Surv. Ophthalmol. 48 (2003) S21–S24.
[33] P. Lewczuk, M. Hasselblatt, H. Kamrowski-Kruck, A. Heyer, C. Unzicker, A.L. Siren, H. Ehrenreich, Survival of hippocampal neurons in culture upon hypoxia: effect of erythropoietin, NeuroReport 11 (2000) 3485–3488.
[34] E. Morishita, S. Masuda, M. Nagao, Y. Yasuda, R. Sasaki, Erythropoietin receptor is expressed in rat hippocampal and cerebral cortical neurons, and erythropoietin prevents in vitro glutamate-induced neuronal death, Neuroscience 76 (1997) 105–116.
[35] J.L. Mosinger, J.W. Olney, Photothrombosis-induced ischemic neuronal degeneration in the rat retina, Exp. Neurol. 105 (1989) 110–113.
[36] J.L. Mosinger, M.T. Price, H.Y. Bai, H. Xiao, D.F. Wozniak, J.W. Olney, Blockade of both NMDA and non-NMDA receptors is required for optimal protection against ischemic neuronal degeneration in the in vivo adult mammalian retina, Exp. Neurol. 113 (1991) 10–17.
[37] S. Mukai, H.K. Mishima, K. Shoge, M. Shinya, K. Ishihara, M. Sasa, Existence of ionotropic glutamate receptor subtypes in cultured rat retinal ganglion cells obtained by the magnetic cell sorter method and inhibitory effects of 20-hydroxyecdysone, a neurosteroid, on the glutamate response, Jpn. J. Pharmacol. 89 (2002) 44–52.
[38] U. Napankangas, N. Lindqvist, D. Lindholm, F. Hallbook, Rat retinal ganglion cells upregulate the pro-apoptotic BH3-only protein Bim after optic nerve transection, Brain Res. Mol. Brain Res. 120 (2003) 30–37.
[39] A.H. Neufeld, Nitric oxide: a potential mediator of retinal ganglion cell damage in glaucoma, Surv. Ophthalmol. 43 (1999) 129–135.
[40] Y. Otori, J.Y. Wei, C.J. Barnstable, Neurotoxic effects of low doses of glutamate on purified rat retinal ganglion cells, Invest. Ophthalmol. Visual Sci. 39 (1998) 972–981.
[41] C.B. Phifer, L.M. Terry, Use of hypothermia for general anesthesia in preweanling rodents, Physiol. Behav. 38 (1986) 887–890.
[42] G.V. Putcha, S. Le, S. Frank, C.G. Besirli, K. Clark, B. Chu, S. Alix, R.J. Youle, A. LaMarche, A.C. Maroney, E.M. Johnson Jr., JNK-mediated BIM phosphorylation potentiates BAX-dependent apoptosis, Neuron 38 (2003) 899–914.
[43] C. Romano, M.T. Price, T. Almli, J.W. Olney, Excitotoxic neurodegeneration induced by deprivation of oxygen and glucose in isolated retina, Invest. Ophthalmol. Visual Sci. 39 (1998) 416–423.
[44] Y. Sadamoto, K. Igase, M. Sakanaka, K. Sato, H. Otsuka, S. Sakaki, S. Masuda, R. Sasaki, Erythropoietin prevents place navigation disability and cortical infarction in rats with permanent occlusion of the middle cerebral artery, Biochem. Biophys. Res. Commun. 253 (1998) 26–32.
[45] T. Saitoh, H.K. Mishima, K. Shoge, K. Ishihara, M. Sasa, Protection against glutamate neurotoxicity in retinal cultures by acidic conditions, Jpn. J. Pharmacol. 76 (1998) 87–95.
[46] M. Sakanaka, T.C. Wen, S. Matsuda, S. Masuda, E. Morishita, M. Nagao, R. Sasaki, In vivo evidence that erythropoietin protects neurons from ischemic damage, Proc. Natl. Acad. Sci. U. S. A. 95 (1998) 4635–4640.
[47] M. Schwartz, E. Yoles, Optic nerve degeneration and potential neuroprotection: implications for glaucoma, Eur. J. Ophthalmol. 9 (1999) S9–S11.
[48] F. Sennlaub, Y. Courtois, O. Goureau, Inducible nitric oxide synthase mediates retinal apoptosis in ischemic proliferative retinopathy, J. Neurosci. 22 (2002) 3987–3993.
[49] T. Shinjyo, R. Kuribara, T. Inukai, H. Hosoi, T. Kinoshita, A. Miyajima, P.J. Houghton, A.T. Look, K. Ozawa, T. Inaba, Down-regulation of Bim, a proapoptotic relative of Bcl-2, is a pivotal step in cytokine-initiated survival signaling in murine hematopoietic progenitors, Mol. Cell. Biol. 21 (2001) 854–864.
[50] K. Shoge, H.K. Mishima, S. Mukai, M. Shinya, K. Ishihara, M. Kanno, M. Sasa, Rat retinal ganglion cells culture enriched with the magnetic cell sorter, Neurosci. Lett. 259 (1999) 111–114.
[51] K. Shoge, H.K. Mishima, T. Saitoh, K. Ishihara, Y. Tamura, H. Shiomi, M. Sasa, Attenuation by PACAP of glutamate-induced neurotoxicity in cultured retinal neurons, Brain Res. 839 (1999) 66–73.
[52] A.D. Sinor, D.A. Greenberg, Erythropoietin protects cultured cortical neurons, but not astroglia, from hypoxia and AMPA toxicity, Neurosci. Lett. 290 (2000) 213–215.
[53] A.L. Siren, M. Fratelli, M. Brines, C. Goemans, S. Casagrande, P. Lewczuk, S. Keenan, C. Gleiter, C. Pasquali, A. Capobianco, T. Mennini, R. Heumann, A. Cerami, H. Ehrenreich, P. Ghezzi, Erythropoietin prevents neuronal apoptosis after cerebral ischemia and metabolic stress, Proc. Natl. Acad. Sci. U. S. A. 98 (2001) 4044–4049.
[54] T. Tabira, Y. Konishi, F. Gallyas Jr., Neurotrophic effect of hematopoietic cytokines on cholinergic and other neurons in vitro, Int. J. Dev. Neurosci. 13 (1995) 241–252.
[55] K. Takahata, H. Katsuki, T. Kume, D. Nakata, K. Ito, S. Muraoka, F. Yoneda, S. Kashii, Y. Honda, A. Akaike, Retinal neuronal death induced by intraocular administration of a nitric oxide donor and its rescue by neurotrophic factors in rat, Invest. Ophthalmol. Visual Sci. 44 (2003) 1760–1766.
[56] M. Tamatani, S. Ogawa, Y. Niitsu, M. Tohyama, Involvement of Bcl-2 family and caspase-3-like protease in NO-mediated neuronal apoptosis, J. Neurochem. 71 (4) (1998) 1588–1596.
[57] M. Tamatani, S. Ogawa, G. Nunez, M. Tohyama, Growth factors prevent changes in Bcl-2 and Bax expression and neuronal apoptosis induced by nitric oxide, Cell Death Differ. 5 (10) (1998) 911–919.
[58] Y. Tsumamoto, K. Yamashita, M. Takumida, K. Okada, S. Mukai, M. Shinya, H. Yamashita, H.K. Mishima, In situ localization of nitric oxide synthase and direct evidence of NO production in rat retinal ganglion cells, Brain Res. 933 (2002) 118–129.
[59] J.H. Weishaupt, G. Rohde, E. Polking, A.L. Siren, H. Ehrenreich, M. Bahr, Effect of erythropoietin axotomy-induced apoptosis in rat retinal ganglion cells, Invest. Ophthalmol. Visual Sci. 45 (2004) 1514–1522.
[60] J. Whitfield, S.J. Neame, L. Paquet, O. Bernard, J. Ham, Dominant-negative c-Jun promotes neuronal survival by reducing BIM expression and inhibiting mitochondrial cytochrome *c* release, Neuron 29 (2001) 629–643.
[61] D. Wu, W.M. Pardridge, Neuroprotection with noninvasive neurotrophin delivery to the brain, Proc. Natl. Acad. Sci. U. S. A. 96 (1999) 254–259.
[62] W. Zhu, G.N. Bijur, N.A. Styles, X. Li, Regulation of FOXO3a by brain-derived neurotrophic factor in differentiated human SH-SY5Y neuroblastoma cells, Brain Res. Mol. Brain Res. 126 (2004) 45–56.
[63] A.B. Zubrow, M. Delivoria-Papadopoulos, Q.M. Ashraf, J.R. Ballesteros, K.I. Fritz, O.P. Mishra, Nitric oxide-mediated expression of Bax protein and DNA fragmentation during hypoxia in neuronal nuclei from newborn piglets, Brain Res. 954 (1) (2002) 60–67.

A Robust Algorithm for Copy Number Detection Using High-Density Oligonucleotide Single Nucleotide Polymorphism Genotyping Arrays

Yasuhito Nannya,[1] Masashi Sanada,[1] Kumi Nakazaki,[1] Noriko Hosoya,[1] Lili Wang,[1] Akira Hangaishi,[1] Mineo Kurokawa,[1] Shigeru Chiba,[1,2] Dione K. Bailey,[4] Giulia C. Kennedy,[4] and Seishi Ogawa[1,3,5]

[1]Departments of Hematology/Oncology, [2]Cell Therapy/Transplantation Medicine, and [3]Regeneration Medicine for Hematopoiesis, Graduate School of Medicine, University of Tokyo, Tokyo, Japan; [4]Affymetrix, Inc., Santa Clara, California; and [5]Core Research for Evolutional Science and Technology of Japan Science and Technology Corporation, Saitama, Japan

Abstract

We have developed a robust algorithm for copy number analysis of the human genome using high-density oligonucleotide microarrays containing 116,204 single-nucleotide polymorphisms. The advantages of this algorithm include the improvement of signal-to-noise (S/N) ratios and the use of an optimized reference. The raw S/N ratios were improved by accounting for the length and GC content of the PCR products using quadratic regressions. The use of constitutional DNA, when available, gives the lowest SD values (0.16 ± 0.03) and also enables allele-based copy number detection in cancer genomes, which can unmask otherwise concealed allelic imbalances. In the absence of constitutional DNA, optimized selection of multiple normal references with the highest S/N ratios, in combination with the data regressions, dramatically improves SD values from 0.67 ± 0.12 to 0.18 ± 0.03. These improvements allow for highly reliable comparison of data across different experimental conditions, detection of allele-based copy number changes, and more accurate estimations of the range and magnitude of copy number aberrations. This algorithm has been implemented in a software package called Copy Number Analyzer for Affymetrix GeneChip Mapping 100K arrays (CNAG). Overall, these enhancements make CNAG a useful tool for high-resolution detection of copy number alterations which can help in the understanding of the pathogenesis of cancers and other diseases as well as in exploring the complexities of the human genome. (Cancer Res 2005; 65(14): 6071-9)

Introduction

Genome-wide detection of copy number alterations has been drawing increasing attention in the field of cancer research as well as in the diagnosis of rare congenital disorders (1–3). In addition to studying genomic alterations in disease, the recent discovery of large-scale copy number variations in the genome of normal individuals has stimulated interest in elucidating their role in the evolution of the human genome (4, 5).

The initial approach to genome-wide detection of copy number changes was comparative genomic hybridization (CGH; ref. 6). This approach first enabled the exploration of genetic alterations in cancers across the human genome at ~20 Mb resolution, and was later improved to less than 1 Mb resolution by replacing target metaphase spreads with a large number of discrete genomic or cDNA clones in arrays (array-based CGH; refs. 1–3). Further increase in resolution was obtained by arrays consisting of 32,433 BAC clones spanning the entire human genome, resulting in comprehensive analyses of cancer genomes at less than 100 kb resolution (7).

Another recently described approach to genome-wide copy number detection is the use of synthetic high-density oligonucleotide microarrays (8–15). These commercially available microarrays, designed to genotype 10,000, 50,000, or 100,000 single-nucleotide polymorphisms (SNP) in human genomic DNA, provide attractive alternatives to BAC-array CGH (16–19). The Affymetrix GeneChip Mapping 100K high-density oligonucleotide arrays contain 116,204 SNPs with a mean spacing of 23.6 kb, and a potential to provide the highest resolution of copy number detection currently available (19). These arrays provide clear technical advantages including robust single-primer assay methodology, accurate and reproducible genotyping, and copy-neutral loss of heterozygosity (LOH) detection compared with array-CGH, karyotyping, and other oligonucleotide CGH arrays. Furthermore, these arrays are manufactured under stringent quality control procedures. However, there are a limited number of algorithms/software available and they suffer from certain limitations which may result in false-positive and false-negative estimations. For example, the software dChipSNP[6] requires the use of a paired-normal sample, which is often unavailable, to perform the analysis (10, 20). Furthermore, dChipSNP can currently only process the Mapping 10K array and not the 50K or 100K arrays. Another alternative software/algorithm for detecting copy number changes from the Mapping 100K arrays is Chromosome Copy Number Analysis Tool (CNAT).[7] CNAT uses a set of 110 normal reference individuals and thus overcomes the paired-normal requirement but does not account for experimental variation in the samples being compared (9).

Here we present an improved algorithm for copy number detection using Affymetrix GeneChip Mapping 100K arrays. This algorithm improves signal-to-noise (S/N) ratios by reducing variation in the raw signal ratios and optimizes the selection of the reference. In addition, availability of accurate genotyping information further enables LOH inference and allele-based copy number analysis. This combination of >100,000 SNP markers and

Note: Supplementary data for this article are available at Cancer Research Online (http://cancerres.aacrjournals.org/).

Requests for reprints: Seishi Ogawa, Department of Regeneration Medicine for Hematopoiesis, Graduate School of Medicine, University of Tokyo, 7-3-1 Hongo, Bunkyo-ku, Tokyo 113-8655, Japan. Phone: 813-3815-5411, ext. 35609; Fax: 813-5804-6261; E-mail: sogawa-tky@umin.ac.jp.

[6] http://www.biostat.harvard.edu/complab/dchip/snp/

[7] http://www.affymetrix.com/support/developer/tools/affytools.affx

a robust copy number algorithm results in a powerful system for high-resolution analysis of copy number alterations, which is unattainable by other current methods.

Materials and Methods

Samples. We obtained the lung cancer cell lines CRL-5929, CRL-5872, and their immortalized lymphoblast CRL-5969, and CRL-5958, from American Type Culture Collection (Rockville, MD), and glioma cell line U251, and immature T-cell line HPB-ALL from Riken (Tsukuba, Japan). Peripheral blood samples and primary tumor specimens were collected from 96 normal volunteers and 33 patients with hematologic malignancies, and subjected to DNA extraction. Informed consent was obtained from the subjects according to the protocols approved by the Institutional Review Boards of the University of Tokyo.

Affymetrix platform. Array experiments were done according to the standard protocols for Affymetrix GeneChip Mapping 100K arrays (Affymetrix, Inc., Santa Clara, CA). Briefly, total genomic DNA was digested with a restriction enzyme (*Xba*I or *Hin*dIII), ligated to an appropriate adapter for each enzyme, and subjected to PCR amplification using a single primer. After digestion with DNase I, the PCR products were labeled with a biotinylated nucleotide analogue using terminal deoxynucleotidyl transferase and hybridized to the microarray. Hybridized probes were captured by streptavidin-phycoerythrin conjugates and the array was scanned and genotypes called as described (18).

Compensation of raw signal ratios and construction of the best-fit reference. Sum of signals from the 10 perfect match probes for the A allele (PA) and those for the B allele (PB) is normalized for each SNP. The mean signal intensity of all autosomal SNPs becomes the same for the two arrays being compared. Relative copy number at the ith SNP locus between the two samples is estimated from the log 2 ratio of the normalized signals of the ith SNP in sample 1 (S_i^{sample1}) and sample 2 (S_i^{sample2}), $\Lambda_i^{1,2} = \log_2(S_i^{\text{sample1}} / S_i^{\text{sample2}})$. For the purpose of compensation for different PCR conditions, it is convenient to write the observed $\Lambda_i^{1,2}$ as the sum of two components (see Supplementary Methods),

$$\Lambda_i^{1,2} = {}^{c}\Lambda_i^{1,2} + p(x)$$

where ${}^{c}\Lambda_i^{1,2}$ represents the corrected copy number and $p(x)$ represents PCR amplification kinetics. We empirically showed that $p(x)$ can be written as

$$p(x) = \sum_{j=1}^{2} (a_j + b_j x_j + c_j x_j^2)$$

where x_1 and x_2 represent the length and GC content of the fragment that contains SNP, and coefficients a_1, a_2, b_1, b_2, c_1, and c_2 should be determined by a series of linear regressions from the observed log 2 ratios. This compensation provides a more accurate estimate of copy number, ${}^{c}\Lambda_i^{1,2}$, which shows a lower SD than original $\Lambda_i^{1,2}$. For a given sample ζ, the averaged best-fit m references, $S_{i,m}^{\text{REF}}$, is calculated as $1 / m(\Sigma_j 2^{{}^{c}\Lambda_{i,j,\zeta}} \times S_i^{\zeta})$, where j (1, 2,..., m) represents the m reference samples in which the SD of ${}^{c}\Lambda_i^{\zeta,j}$ takes the lowest values. The log 2 ratios of S_i^{ζ} for this reference, ${}^{c}\Lambda_i^{\zeta,\text{REF}}$, are evaluated for their variance and give a better inference of copy number at the ith locus. Following the first round normalization, compensations, and optimization of references thus far described, the second-round adjustment is done for the analysis of tumor samples having complex chromosomal abnormalities for accurate calculation of the regression curves and correct assignment of the ploidy, because the mean log 2 ratio does not conform to that for the diploid SNPs and determination of the regression curves using all autosomal SNPs is confounded by a large number of nondiploid SNPs. In the latter process, we set chromosome numbers in accordance with the ploidy information referred by previous literature or determined by other methods, including fluorescence *in situ* hybridization, then iteratively performed the second-round normalization, compensations, and selection of optimal references exclusively using only such SNPs that belong to the diploid region for determination of the coefficients required for this step.

Allele-based analysis using a paired normal sample. When a paired normal sample is used for the allele-based copy number estimate, analysis is confined to those SNPs of which genotype in the reference is AB (heterozygous) and signal sums of PAs (${}^{A}S_i$) and PBs (${}^{B}S_i$) for the ith SNP are taken separately both in the tumor and the reference. The log 2 ratios of normalized values, ${}^{A}S_i$ and ${}^{B}S_i$, are similarly compensated for the different experimental conditions to calculate the corrected log 2 ratios, ${}^{c}\Lambda_i^{\text{tumor, REF}}(A)$ for PAs and ${}^{c}\Lambda_i^{\text{tumor, REF}}(B)$ for PBs, where the coefficients used for the normalization and compensation procedure are determined using all the SNPs in a region specified as diploid as is the case with analysis using references not derived from the same individual. For the purpose of allele-based copy number analysis, the corrected log 2 ratios for the heterozygous SNPs are separated in two groups,

$$\Lambda_{\max} = \{x \mid \max\{{}^{c}\Lambda_i^{\text{tumor,ref}}(A), {}^{c}\Lambda_i^{\text{tumor,ref}}(B)\}\}$$

$$\Lambda_{\min} = \{x \mid \min\{{}^{c}\Lambda_i^{\text{tumor,ref}}(A), {}^{c}\Lambda_i^{\text{tumor,ref}}(B)\}\}$$

To obtain the allele-based copy number view, the members of each group are rearranged in the genetic order and plotted as shown in Fig. 5 (*middle*).

Copy number inference. Although compensation for difference in PCR conditions and optimization of the reference significantly reduce the deviation of log 2 ratios, further elimination of random noise greatly helps visualization of copy numbers along the chromosomes and efficient detection of copy number alterations. In "local mean analysis," the sequence of the mean log 2 ratios, ${}^{c}\bar{\Lambda}_{i,k}^{\text{test, REF}} = 1/k \sum_i^{i+k-1} {}^{c}\Lambda_i^{\text{test, REF}}$, is calculated, where k is the number of terms to be averaged and arbitrarily set to 3 to 10, according to the SD values after compensations of log 2 ratios and optimization of nonreferences for diploid SNPs. In the alternative analysis using a hidden Markov model (21), the inference of copy number is more efficient and automated, in which a real state of the copy number sequence (a hidden state) along a chromosome is inferred from the observed sequence ${}^{c}\Lambda_i^{\text{test, REF}}$ as the state of maximum likelihood that is calculated from the state transition load and the probability of the hidden state to "emit" the observed sequence of log 2 ratios, using the Viterbi algorithm. We assumed that copy number change (state transition) is the result of a genetic recombination event between the two adjacent SNP loci, and Kosambi's map function $(1/2)\tanh(2\theta)$ is used to transform the genomic distance, or recombination fraction between the two SNPs (θ) to state "transition probability," where θ is expressed in cM units; for simplicity, 1 cM should be 1 Mbp. The observed log 2 ratio is assumed to follow the normal distribution according to real copy number states, which gives the "emission probability." The variables of normal distribution were empirically determined from the experimental data (Supplementary Methods).

Comparison and confirmation of the results. CNAT was executed following the instructions of the suppliers. For proper comparison with our system, log 2–converted values of the Genome Smoothed Analysis Copy Number (GSA_CN) were compared. FISH analyses were done as previously described (13). Probe information used in FISH analysis is supplied in Supplementary Table 1. PCR primers were designed to amplify several adjacent fragments that are within and outside of the homozygously deleted regions in tumor samples. Primers and PCR conditions are provided in Supplementary Table 2.

Copy Number Analyzer for Affymetrix GeneChip mapping 100K arrays. Copy Number Analyzer for Affymetrix GeneChip Mapping 100K arrays (CNAG) ver 1.0 is the implementation of the set of algorithms described above that is written in C++ for Microsoft Windows. All the examples of copy number analysis with Affymetrix GeneChip Mapping 100K arrays presented in this article were done using CNAG. All data used in this article and CNAG can be downloaded.[8]

[8] http://www.genome.umin.jp

Results

Reduction of signal-to-noise ratio. To allow for high-fidelity copy number estimation from genotype arrays, we evaluated several variables that influence signal intensity between arrays being compared. By taking into account these variables, erroneous copy number changes can be eliminated. Initially, the raw signal intensities between normal DNA samples were compared. An arithmetic sum of the hybridization signals from all perfect match probes for each SNP was normalized so that the mean signal intensity of all autosomal SNPs becomes the same for the two arrays. Next, SDs of log 2 ratios of the normalized signals were calculated for each SNP locus and compared for

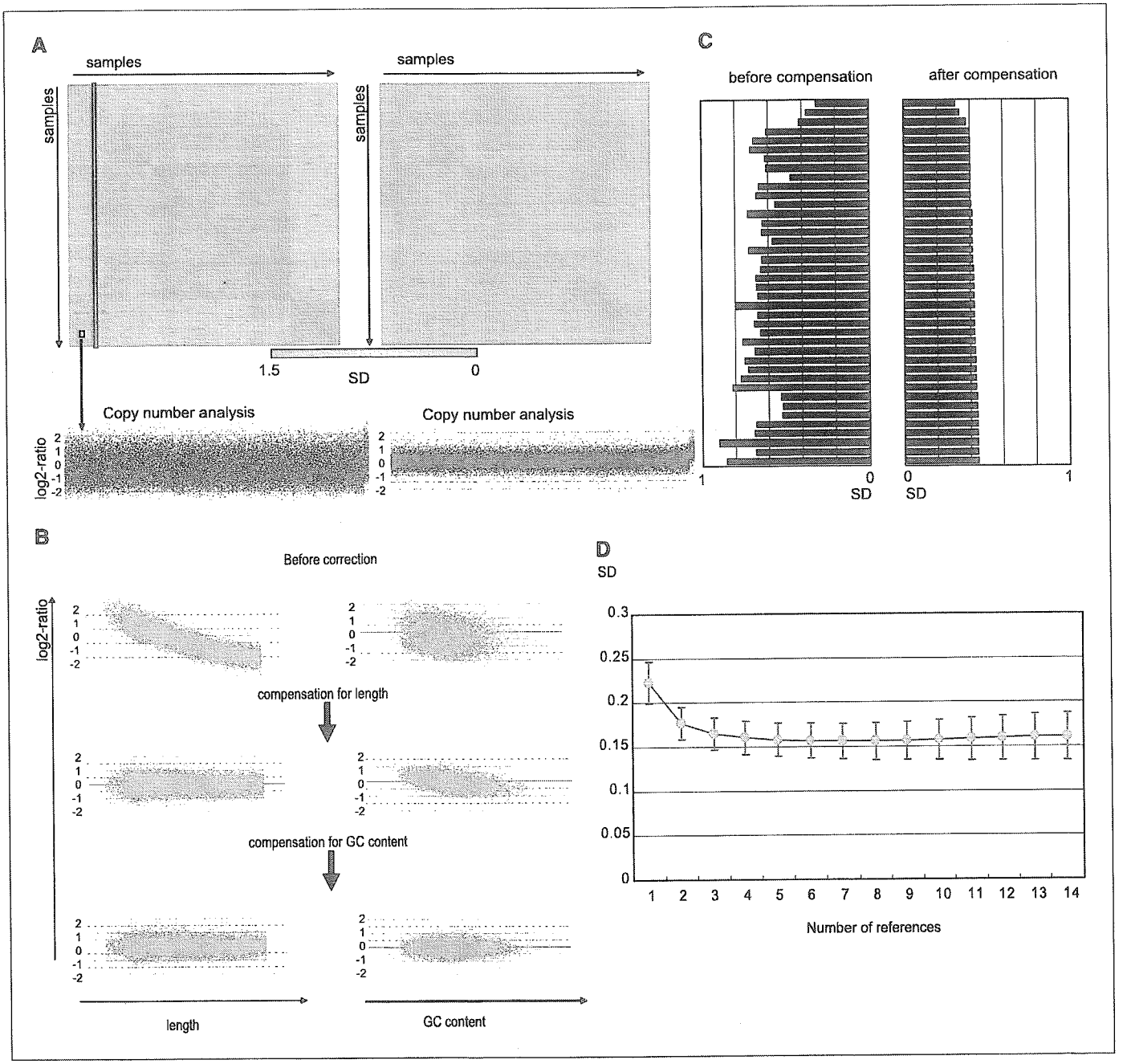

Figure 1. *A*, SDs of log 2 ratios for all autosomal SNPs were calculated for all combinations of array data from 96 normal individuals before (*left matrix*) and after (*right matrix*) compensations, and color coded according to the SD values. The array data are arranged in the order of experiments. Significant variations in SD values are found between different array data before compensations, whereas combinations of samples that were processed together tend to form clusters showing low SD values. After compensations, the variations in SD values among different combination become less conspicuous. Log 2 ratios corresponding to the indicated cell before and after compensations are plotted in the chromosomal order (*bottom*). *B*, compensations of log 2 ratios for dissimilar PCR conditions between test (sample 103) and reference (sample 308) arrays. Log 2 ratios are plotted against length (*right*) and GC content (*left*) of the restriction fragment to which each SNP belongs, before compensations (*top*), after the first compensation for fragment length (*middle*), and after the second for GC content (*bottom*). Dependence of log 2 ratios on fragment length and GC content is serially resolved after compensations with the consequent reduction in the SD value. *C*, effects of compensations on SD. SD values for varying combinations of a fixed array [sample 110, *blue rectangle* in *A* (*left*)] with different arrays are significantly reduced after compensations. *D*, effects of using the best-fit multiple references on reduction in SD values. The mean SD values were calculated using an increasing number of the best-fit references for 96 normal samples and plotted with SEs against the number of references averaged.

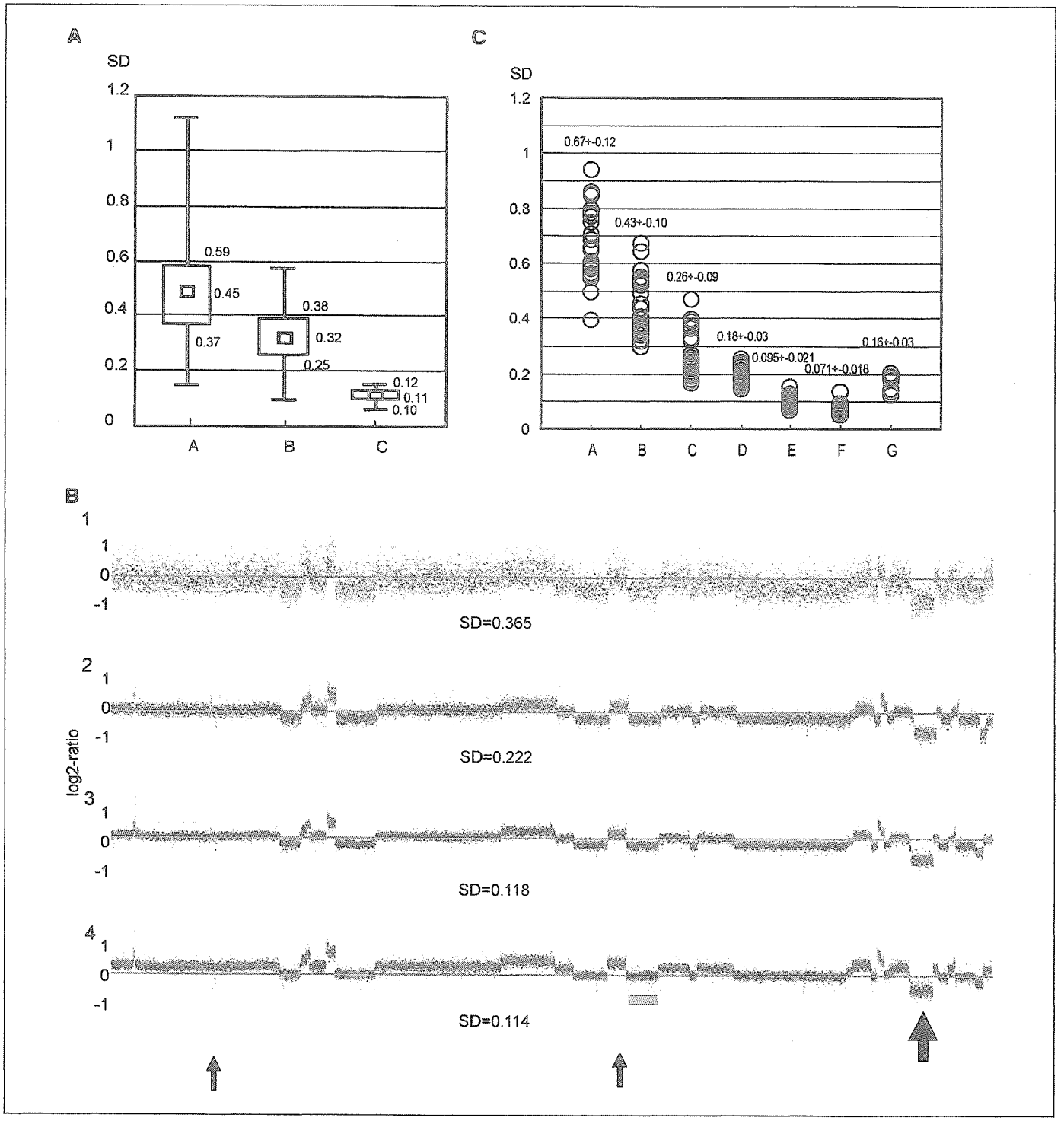

Figure 2. *A,* mean SD value of log 2 ratios and 25th and 75th quartiles are calculated for all combinations of 96 normal samples, before (raw log 2 ratios; *lane A*) and after compensations (*lane B*) for dissimilar PCR conditions ($N = {}_{96}C_2$). The calculations were also done after using the five best-fit references (lane C). *B,* genomic DNA from a glioma cell line U251 was analyzed for copy number alterations with or without compensations for different experimental conditions using different compensation algorithms. The raw log 2 ratios in the chromosomal order show widely fluctuated baselines (*1*; SD = 0.365), which are greatly reduced after compensation of experimental conditions and using the best-fit single (*2*; SD = 0.222) and multiple references (*3*; SD = 0.118). Regions of homozygous and hemizygous deletion are indicated by small and large arrows. The SD value is further decreased (SD = 0.114) when the second round compensation procedures are applied by specifying a region of diploid alleles (*4, red bar*). With this approach, diploid regions as well as other regions showing varying ploidy states are correctly assigned to their real ploidy. For proper comparison, SD values are calculated for the SNPs within the diploid range (*red bar*). *C,* SD values were also calculated and plotted for 33 tumors samples compared with a representative normal sample (sample 101) before (*lane A*) and after compensations using a single best-fit reference (*lane B*), after analysis with the average of the five best-fit references (*lane C*). The regression curves for compensations were determined using all autosomal SNPs (*lanes A-C*) or exclusively using those within a diploid region arbitrarily selected by visual inspections of the copy number output from previous steps (*lane D*). After a series of compensations and optimization of references, the average of log 2 ratios of every set of consecutive five (*lane E*) or ten (*lane F*) SNPs in the genetic order was taken to further reduce persisting background noises (local mean analysis; see Materials and Methods). SD values calculated using a paired normal reference with no local averages are also provided (*lane G*).

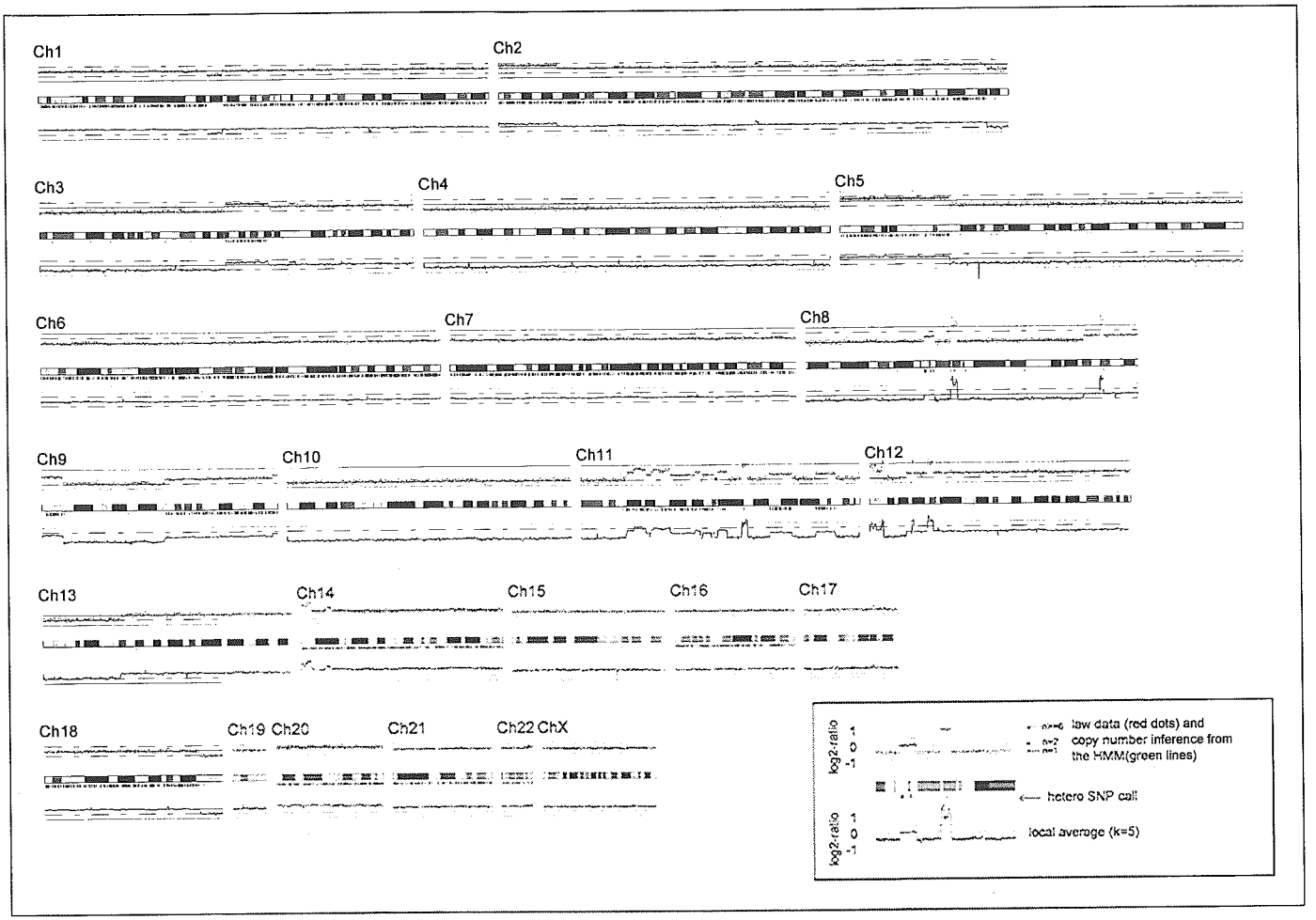

Figure 3. Analysis of CRL-5929 using five best-fit references and the whole genome result. *Red dots*, raw log 2-ratio values for each SNPs. Copy number inferences from a hidden Markov model (*green lines*) and local mean analysis for five consecutive SNPs (*blue curves*) are appended. Heterozygous SNP calls are marked with green bar lines beneath the chromosomes.

every combination of two arrays from 96 normal individuals (see Materials and Methods). This resulted in a considerable difference in SD values among different combinations of samples (Fig. 1*A* (*left*) and Supplementary Fig. 1). We hypothesized that different PCR kinetics among experiments could be the origin of these highly variable SD values and that adjusting for these experimental variables may allow for more accurate comparisons (Supplementary Methods). It should be noted from the block-like structures of the SD graph that the behavior of SD values is largely determined by the group of experiments done together, rather than the individual experiments.

To assess the dependence of the log 2 ratios of signals on PCR kinetics, we plotted log 2 ratios against several variables that may affect PCR reactions in different experiments, including length of PCR fragments and GC content (Fig. 1*B*). By compensating for the effects of these variables using two-step quadratic regressions, the log 2 ratios almost completely offset the dependencies of log 2 ratios on these variables and the SD value between the given two experiments is reduced from 0.88 to 0.40 (Fig. 1*B* and *C*). In fact, these compensation procedures dramatically improve the distribution of SD values among 96 normal samples, enabling comparisons across different samples or groups of experiments (Fig. 1*A*, *right*). SNPs located on fragments shorter than 500 bp, which account for 2.9% of total SNPs, tend to be resistant to these compensations and were precluded from the analyses altogether.

Optimization of reference selection. Although correcting for the fragment length and GC content dramatically reduces SD values, there was still considerable variation among different samples. Therefore, we explored the effects of using different reference sets. The type of reference set used largely depends on the following: (*a*) cases where tumor and normal DNA are available from the same patient (paired normal samples) and (*b*) cases where only the test or tumor sample is available. Use of a paired normal sample coupled with compensation for variability across experimental conditions generally gives lower SD values. However, the benefit of having a paired normal sample for a reference tends to be diminished when test and reference samples are processed separately (data not shown). The case when a paired normal sample for a reference is unavailable is more complicated. Although the array that shows the lowest SD value for the test sample is a candidate for the reference, we investigated choosing the average of multiple samples with the lowest SD values or best-fit samples as a reference.

To determine the effect of averaging multiple references on SD values, data from 96 normal samples were compared with the averages of varying numbers of the best-fit references, and SD values were calculated for each comparison (Fig. 1*D*). As the number of samples increases to five, the SD value gradually decreases to <0.15

for most normal samples and then reaches a plateau, suggesting that taking an average of at least five best-fit samples is sufficient to optimize the comparison (Fig. 2*A*).

A direct comparison of the copy number estimation using a paired normal reference and best-fit reference was also evaluated for a small cell carcinoma cell line (CRL-5929). The results using a paired normal reference show a slightly lower SD value (0.141 versus 0.177) and smaller fluctuations of baselines than with the best-fit multiple references (Supplementary Fig. 2*A*). However, copy number inference from the hidden Markov model (see Materials and Methods) analysis and local averaging gives an equivalent result (Supplementary Fig. 2*B*). This suggests that the multiple best-fit references are an excellent substitute in cases where a constitutional paired normal reference is not available.

Validation of new algorithm using normal and tumor samples. We evaluated the performance of this new algorithm by analyzing a variety of samples. Figure 2*B* shows a representative analysis of a glioma specimen, showing the dramatic reduction of baseline fluctuations or SD values when using this algorithm relative to raw log 2 ratios. The raw data (Fig. 2*B*-1) has an SD of 0.365, which is reduced to 0.222 after applying a single best-fit reference (Fig. 2*B*-2). A further improvement was seen when using multiple best-fit references, SD = 0.118 (Fig. 2*B*-3). Regions of homozygous and hemizygous deletion are indicated by small and large arrows, respectively. As tumor samples frequently exhibit complex chromosome abnormalities with extensive genetic imbalances (22), analysis of tumor specimens requires additional considerations in selection of references. SD values may be disproportionately inflated or overwhelmed by the effect of genetic abnormalities when all autosomal signals are included in the calculation of SD values. To circumvent this problem and to calculate proper SD values for reference selection, we adopted a two-step approach. We first made a tentative estimation of the copy number changes by using all autosomal signals and predicted the regions that are diploid by reference to other independent information (FISH, PCR, or results in the literature). In the second step, one of these diploid regions was used for normalization and for calculation of SD values to identify the best-fit references. This final step further improved the SD value, 0.114 (Fig. 2*B*-4).

Reductions of SD values in different tumor samples are summarized in Fig. 2*C*. The SD values from 33 tumor samples were calculated from raw data, as well as using the new algorithm with five best-fit references. The distribution of SD values is clearly decreased using the new algorithm. Figure 2*C* also illustrates the results using limited regional SNPs, local averaging of five or ten consecutive SNPs, and using a paired normal reference. After all corrections and optimizations of best-fit reference samples, a local mean procedure was applied which results in lower SD values relative to the paired normal reference sample, where no local mean was used. All of these analyses resulted in a dramatic reduction in the SD values relative to the raw data, which enables genome-wide copy number detection with a high degree of accuracy (Fig. 3).

Sensitivity of copy number analysis using improved algorithm. We evaluated the sensitivity of our copy number detection algorithm by calculating mean log 2 ratios for those regions having known copy number alterations. The observed

Table 1. Comprehensive list of homozygous deletions and gains in tumor cell lines

Sample*	Change	Length (kb)†	Cytoband	SNPs involved	Genes involved	Confirmation‡
CRL-5929	Deletion	5.5-76	5q13.1	4	*PIK3R1*	PCR (ID1)
	Gain	2,253-2,652	8q12.2-8q12.3	146	*ASPH*, *GGH*, others	FISH (RP11-234F8)
	Gain	1,347-1,475	8q24.21	83	*MYC*	FISH (RP11-145G10)
	Gain	1,662-1,771	11q14	113	*ME3*, *SYTL2*, others	FISH (RP11-90K17)
	Gain	566-627	12p13.33	23	*CACNA1C*, *DCP1B*, others	
	Gain	825-919	12p13.32	37	*CCND2*, *PARP11*	
	Gain	2,720-2,780	12p13.31	31	*LAG3*, *GAPD*, others	FISH (RP11-166G2)
	Gain	693-888	12p12.1	39	*SLCO1*, *IAPP*, others	
	Gain	1,925-2,090	12p11	115	*PTHLH*, *MRPS35*, others	FISH (RP11-74J4)
	Gain	609-648	14q11.2	48	*CCNB1IP1*	FISH (RP11-98N22)
	Gain	1,770-1,918	14q11.2	93	*SALL2*, *METTL3*, others	FISH (RP11-70F9)
	Deletion	0.9-29	15q23	3	—	PCR (ID2)
CRL5872	Gain	8,763-10,224	1q21.2-1q22	92	*BCL9*, *IL6R*, others	FISH (RP11-71L20)
	Gain	1,703-2,814	5p15.33	41	*IRX4*, *NDUFS6*	FISH (RP11-20B3)
	Gain	1,183-2,113	8p11.22-8p11.21	43	*INDO*, *ADAM2*	FISH (RP11-262I23)
	Deletion	54-131	9p23	9	—	PCR (ID4)
	Deletion	316-404	9p23	16	—	
	Deletion	391-556	9p22.3	14	*CER1*, *FREM1*	
	Deletion	1,498-1,684	9p22.2	42	*SH3GL2*	
	Deletion	1,237-1,457	9p21.3	44	*IFNA*, *CDKN2A*, others	PCR (ID5)

NOTE: Homozygous deletions ($n = 0$) and high grade gains ($n > 4$) were identified using a hidden Markov model.

*All samples are compared with paired normal references to distinguish between tumor-specific copy number alterations and copy number polymorphisms.

†Minimal size range is the distance of both ends of consecutive SNPs that meet the criteria. Maximal size range is the distance of the SNPs that flank the deleted or amplified regions. Based on UCSC Build 16 (hg16) assembly (http://genome.ucsc.edu/cgi-bin/hgGateway).

‡The probe names used in FISH analysis and the primer set IDs used in PCR analysis are shown in parentheses. See Supplementary Tables 1 and 2 for details.

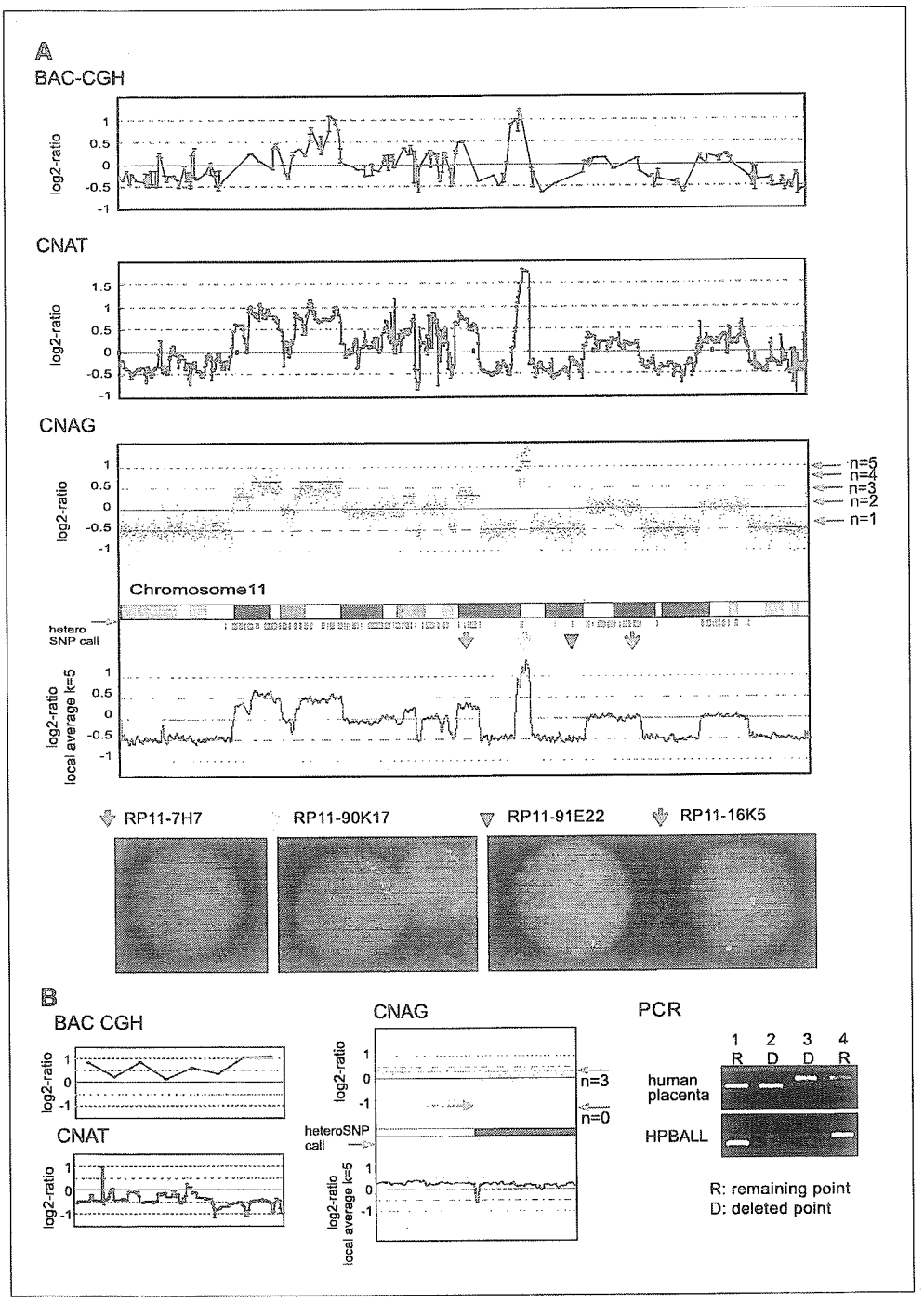

Figure 4. *A*, comparison of BAC array (*top*), CNAT (*middle*), and CNAG (*bottom*). CRL-5969 was used as paired normal reference in all methods. Chromosome 11 is represented. FISH analysis confirmed the detected changes. *B*, immature T-cell line HPB-ALL was examined using BAC-arrays (*left top*), CNAT (*left bottom*), and CNAG (*middle*). CNAG detected a homozygous deletion in 2p16.3 (*red arrow*, position 48,002,999-48,059,096) that was not detected by BAC-array or CNAT. The deletion was confirmed by PCR (*right*). 2p21-2p16.3 is presented for all three methods.

mean log 2 ratio for X chromosomes between 48 males and 48 females was −0.49 (SD = 0.035), which is about half of the expected value (= −1) for the single copy difference (Supplementary Fig. 3). Similarly, the observed mean log 2 ratio for known trisomy in CRL-5929 in chromosome 20[9] was 0.36, compared with the expected value of 0.585. These discrepancies are thought to result from nonspecific background hybridization, which could not be measured and subtracted before taking log 2 ratios, although the background factors can be theoretically estimated and used for performing copy number inference using a hidden Markov model (Supplementary Method). Because the SD value of log 2 ratios for baseline diploid SNPs is 0.18 ± 0.03 with best-fit references or lower with a paired normal reference, the estimated S/N ratio is ~2.0 (for trisomy) or more (for monosomy) in most cases.

Estimation of the resolution is directly proportional to the distribution of SNP markers. We determined the size of genomic alterations in CRL-5929 and CRL-5872 cell lines (Table 1). Deletions of less than 500 kb at 14q11.2 (T-cell receptor α) and less than 393 kb at 7q34 (T-cell receptor β) were observed in the immature T-cell line HPB-ALL; these were caused by a T-cell receptor rearrangement (23). The genomic regions comprising these deletions contain approximately 20 and 10 SNPs, respectively, from the Affymetrix GeneChip Mapping 100K arrays. As the number of SNP markers

[9] http://www.path.cam.ac.uk/~pawefish/LungCellLineDescriptions/NCI-H2171.html